SOFT BIOMIMETIC FINGER WITH TACTILE SENSING AND SENSORY FEEDBACK CAPABILITIES

by
Sriramana Sankar

A thesis submitted to Johns Hopkins University in conformity with the requirements for the degree of Master of Science and Engineering

Baltimore, Maryland

August 2020

Abstract

The compliant nature of soft fingers allows for safe and dexterous manipulation of objects by humans in an unstructured environment. A soft prosthetic finger design with tactile sensing capabilities for texture discrimination and subsequent sensory stimulation has the potential to create a more natural experience for an amputee. In this work, a pneumatically actuated soft biomimetic finger is integrated with a textile neuromorphic tactile sensor array for a texture discrimination task.

The tactile sensor outputs were converted into neuromorphic spike trains, which emulate the firing pattern of biological mechanoreceptors. Spike-based features from each taxel compressed the information and were then used as inputs for the support vector machine (SVM) classifier to differentiate the textures. Our soft biomimetic finger with neuromorphic encoding was able to achieve an average overall classification accuracy of 99.57% over sixteen independent parameters when tested on thirteen standardized textured surfaces. The sixteen parameters were the combination of four angles of flexion of the soft finger and four speeds of palpation. To aid in the perception of more natural objects and their manipulation, subjects were provided with transcutaneous electrical nerve stimulation

(TENS) to convey a subset of four textures with varied textural information. Three able-bodied subjects successfully distinguished two or three textures with the applied stimuli.

This work paves the way for a more human-like prosthesis through a soft biomimetic finger with texture discrimination capabilities using neuromorphic techniques that provides sensory feedback; furthermore, texture feedback has the potential to enhance the user experience when interacting with their surroundings. Additionally, this work showed that an inexpensive, soft biomimetic finger combined with a flexible tactile sensor array can potentially help users perceive their environment better.

Primary Reader and Advisor: Nitish V. Thakor, PhD

Secondary Reader: Marlis Gonzalez-Fernandez, MD, PhD

Dedication

I am dedicating this thesis to my fiancée, mom, and dad for their inspiration and continued support through all my endeavors.

Contents

List of Tables

List of Figures

Chapter 1

Introduction

Interest in soft robotics has grown over the past couple of decades largely due to their compliant structure that tends to be more biomimetic and suitable for tasks like delicate object handling and palpation. Currently, soft robots have been adapted to a variety of areas such as locomotion, minimally invasive surgery, and orthoses [1]–[4]. A variety of soft orthoses have been developed for hand, elbow, and ankle rehabilitation as well as for suction liners, prostheses, and human augmentation systems [5]–[9]. Since soft robots have the potential to mimic organisms and interface with human bodies, there is an increasing trend towards the development of biomimetic robotic grippers and prostheses [8], [10]–[18]. While these designs have a great grasping capacity, most soft fingers have limited dexterity and sensing capabilities. A few soft fingers have independent, interphalangeal actuation producing more than one degree of freedom [15], [19]. However, none have incorporated texture sensing and sensory feedback capabilities. This study attempts to address this need.

The compliant nature of soft robots gives them an advantage over rigid continuum robots because the soft manipulator allows for a more conforming grasp when manipulating objects of diverse sizes, shapes, and texture. Additionally, most soft robots are under-actuated, meaning the degrees of freedom (DOF) do not necessarily correspond to the number of joints. This allows soft robots to have increased complexity and movement without adding additional components [20]. Soft robots are either built using compliant materials such as silicone, polymer, rubber, or combined soft and rigid materials creating endo- or exoskeletons with soft actuators [10], [18], [21]. Due to the prevalence of flexible materials and multiple extruders, many soft robots are 3D-printed without any need for assembly, further reducing the costs [8]. Soft robotic actuators range from pulley systems, pneumatics, to hydraulics [20]. Pneumatic actuators are most common because air is lightweight, omnipresent, and minimally viscous. Given these benefits, this study designed a pneumatically actuated biomimetic finger that is fabricated from silicone and fabric.

When subjects receive static and dynamic sensory cues during tactile sensing, they can understand and dynamically interact with their surroundings. Static cues can be obtained instantaneously, with a few studies incorporating these cues, such as temperature, curvature, and force, into their soft robots [16], [17], [22], [23]. Processing dynamic cues, such as texture, is more complex as it requires spatial and temporal information. The identification of surface texture is a desirable capability using tactile sensing and feedback as an aid to surgeons during minimally invasive surgery [24], [25]. Additionally, tactile sensing has been shown to help prosthesis users with handling everyday objects [26], [27]. This idea of texture recognition was proposed by our group in preliminary studies with soft

robots, particularly in prosthetic applications [28], [29]. Various tactile sensors made from multiple materials have been used for texture discrimination tasks in previous studies [30]–[41]. Several studies tested their sensor and texture discrimination methods on sets of 2-15 grated textures [30]–[36]; while fewer studies used a smaller subset of natural textures [37]–[41]. While these sensors perform fairly well at texture discrimination tasks, they do not use a flexible, textile sensor that is easily incorporable into the soft biomimetic finger. Additionally, most of these sensors do not neuromorphically encode sensory information for texture discrimination.

Neuromorphic encoding is a method to mimic the response of mechanoreceptors found in human skin that transduce tactile information as a neural spike train code. To model biomimetic tactile sensing, encoding, and feedback for our system, it is desirable to understand and model these tactile receptors. This process is inspired by the behavior of neurons in transmitting and processing information. Neuromorphic encoding of the spike train and its subsequent processing is more computationally efficient at encoding spatial and temporal information than standard analog data [33], [37], [42], [43]. Additionally, neuromorphic encoding allows for easier integration with neuroprostheses as the biomimetic spiking activity can be delivered directly to the skin or afferent nerves to elicit more natural sensory perception [44], [45]. Such tactile feedback, mimicking the skin receptors and sensory nerve's code, has the potential to reduce the learning time required for the brain to adapt to using the neuroprosthesis [43]. Neuromorphic encoding and spike-based decoding have been used for texture discrimination tasks in previous studies [30], [37], [46], [47]. However, this study combines the benefits of the soft biomimetic finger

with the integrated flexible, textile tactile sensor and uses neuromorphic encoding with support vector machine (SVM), while also providing users with sensory feedback.

The goal of this work is to demonstrate the texture discrimination capabilities of a novel soft biomimetic finger that is pneumatically actuated and lays the foundation for a prosthetic finger with palpation and sensory feedback capabilities. The work presented here builds on our preliminary studies, where we first presented the prototype design of a soft finger and the use of tactile sensors [28], [29]. Now, in this work, we fully investigate the effects of palpation speed and actuation on texture discrimination using the soft finger and explore the use of sensory feedback (Figure 1.1). This thesis first reviews recent developments in soft robotic prosthesis and texture recognition in prostheses. Then, the comprehensive design of the soft biomimetic finger and the textile tactile sensor array is presented. The tactile sensor response is encoded in a biomimetic manner, mimicking the properties of skin tactile receptors. Then, we test the texture discrimination performance with the SVM classifier and convey the classified texture information to the user using sensory feedback. Finally, the continuing work and future directions are discussed. Our work represents several transformative steps leading to a novel soft biomimetic finger design with a flexible sensor and capability to palpate textures and subsequently provide sensory feedback.

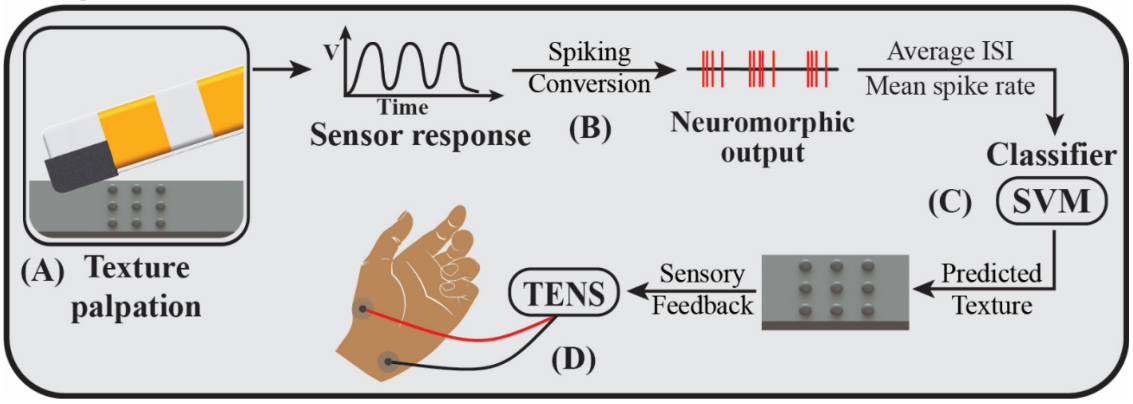

Figure 1.1: Overview of the texture discrimination method using the soft biomimetic finger. (A) Texture palpation using the soft finger with the tactile sensor. (B) The sensor response is neuromorphically encoded using the Izhikevich neuron model, to mimic slowly adapting (SA-1) neuron spiking patterns. (C) The spike-based features, average inter-spike interval (ISI) and mean spike rate, are used as inputs for SVM to classify the textures. (D) Sensory feedback is then provided to the user through transcutaneous electrical stimulation (TENS).

Chapter 2

Review of Soft Robotic Prosthesis

Robots have impacted the way humanity interacts with its environment. Interest in soft robotics has grown over the past couple of decades largely due to their compliant structure that tends to be more biomimetic and suitable for tasks like delicate object handling and palpation. Currently, soft robots have been adapted to a variety of areas such as locomotion, minimally invasive surgery, rehabilitation, and prostheses. Marine-inspired soft robots have been built to navigate aquatic environments [48], [49]. In minimally invasive surgery, soft robots have been used to provide visual aid and palpate for abnormalities in occluded areas [1]–[4]. A variety of soft orthoses have been developed for hand, elbow, and ankle rehabilitation at home, as well as suction liners, 3D printable prosthetics, and even human augmentation systems [5]–[9].

The following section focuses on reviewing soft robots based on their construction and material followed by their sensing capabilities. There has been significant work done on reviewing actuation methods in soft robots [21], [50], [51]. Therefore, this review

chapter will not focus on the different types of actuation. The soft robot that was fabricated and used in this project is a pneumatically actuated soft finger composed mainly of silicone. Further details about the soft biomimetic finger are provided in Chapter 4.1.

2.1 Construction and Material

The structure and function of soft robots depend highly on their construction and materials. Many materials can be used to create functional soft robots, where the method of actuation is often tied to the material choice. The properties of the material such as tensile strength, durability, and response time are important, especially when looking at certain actuation methods. The most used materials are Silicone, 3D printed material, Hydrogels, and Electroactive polymers (EAP), which are discussed in the following sections.

2.1.1 Silicone

Most soft robots are constructed from silicone due to its versatility and low cost. Silicone can be molded and formed into multiple structures and has been widely used widely commercially [52]. They can be used to create pneumatic actuators, robotic grippers, and buckling linear actuators [28], [53]–[63]. However, soft robots constructed from silicone do not have the longevity and resilience provided by rigid materials. Additionally, the drawback of a lot of compliance is that soft robots using silicone tend to buckle and produce limited force when grasping objects, depending on the actuation method.

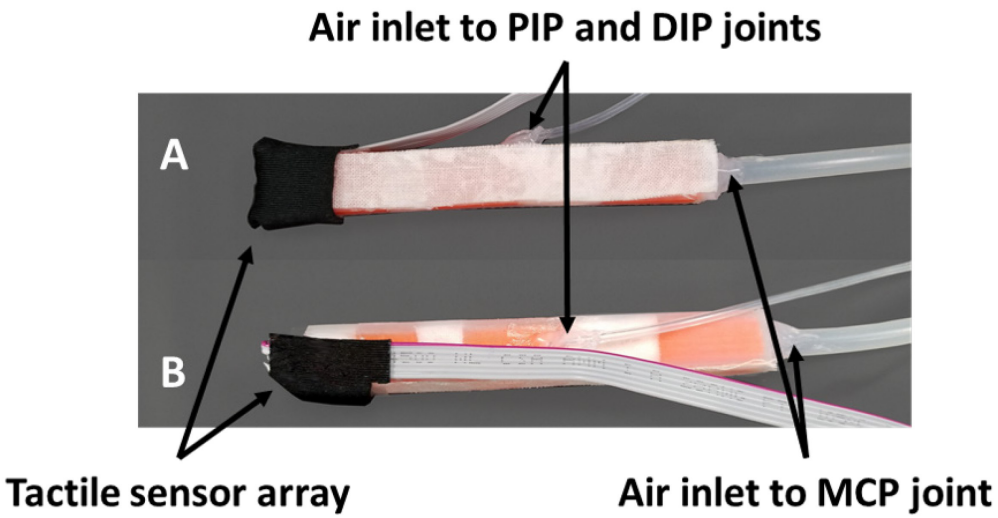

Figure 2.1: Soft biomimetic finger fabricated mainly using silicone [63].

2.1.2 3D printed material

3D printed soft robots benefit from being easily mass-produced by using relatively cheap materials. They can be fabricated with various 3D printing methods such as Fused Deposition Modeling (FDM), Digital Mask Projection Stereolithography (DMP-SL), Selective Laser Sintering (SLS), and Digital Light Projector (DLP) [22], [50], [64]–[69]. These soft robots tend to have a high degree of freedom and can be used to construct pneumatic or fluidic actuators. Generally, the tensile strength of 3D printed soft robots tends to be low, which causes them to break easily. However, better 3D printers and newer advanced materials have been able to improve the 3D printed soft robot's tensile strength [70].

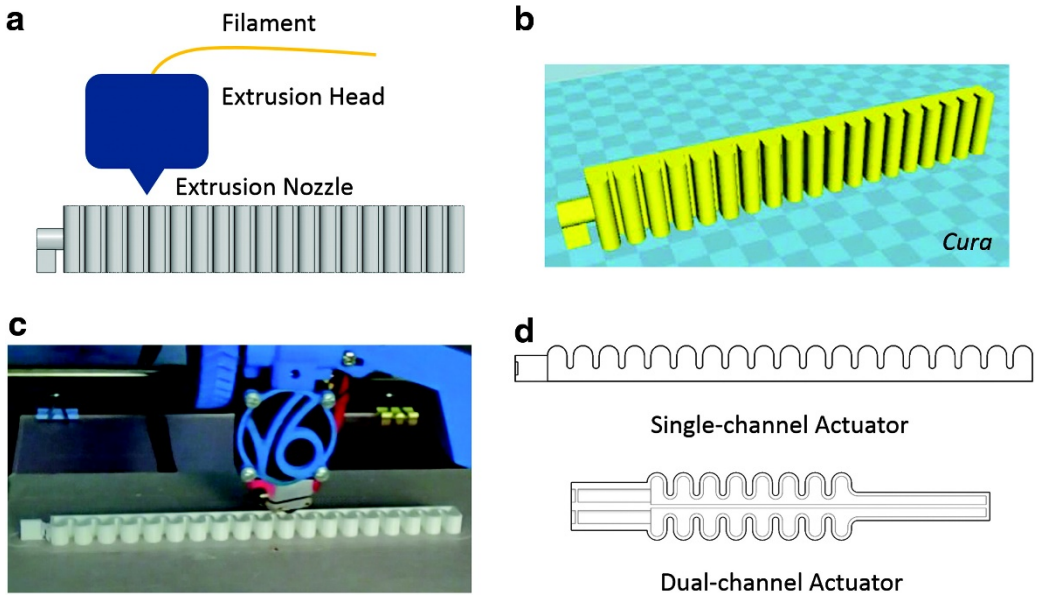

Figure 2.2: (a) Schematic of 3D printed soft robot from (b) STL file to (c) 3D printing using fused deposition modeling (FDM) [65].

2.1.3 Hydrogel

Hydrogels are a network polymer chains that are hydrophilic but highly absorbent. This allows them to hold large quantities of water and maintain their structure while being compliant. The swelling due to water absorption creates the actuation for bending. Hydrogels are easily customizable, have many degrees of freedom, and can be manufactured on a small scale [71]–[75]. However, hydrogel fabrication can be expensive, have low tensile strength, and be difficult to handle.

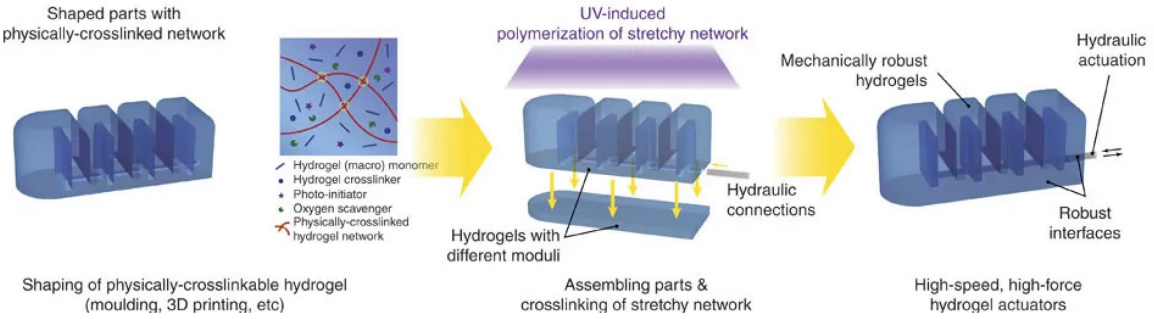

Figure 2.3: Schematic of the fabrication of the hydraulic hydrogel actuators [72].

2.1.4 Active Polymers

Research into active polymers has grown, with Electroactive polymers (EAP) being the most common. When an electric field is applied to EAPs, they change in shape and/size [76]–[78]. They have large compliance and can provide many degrees of freedom (DOF). However, they are very inefficient because they require a high voltage to function and have slow response times.

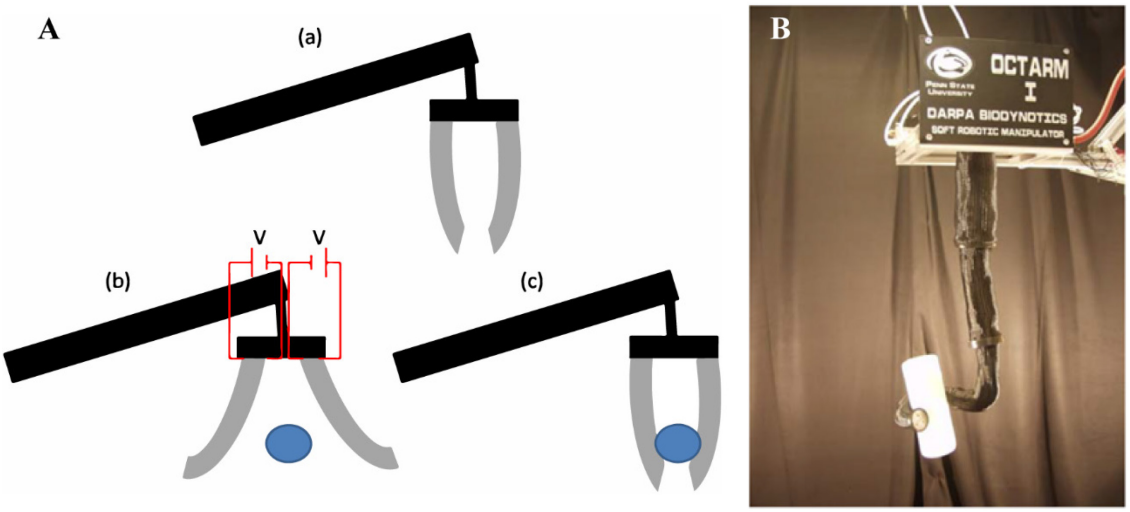

Figure 2.4: (A-a) Graphic demonstrating how electroactive polymers work; (A-b) voltage applied to EAP, which deforms the fingers; (A-c) when voltage is removed, the EAP returns to its original shape [78]. (B) Continuum robot arm inspired by cephalopods using EAPs [76].

Other active polymers such as sheet material, Polydimethylsiloxane (PDMS), and Nitinol are also being developed to construct soft robots. As with EAP, the shape of active polymers changes in response to an external stimulus but regain their original shape once the stimulus is removed. The sheet material can be heat bonded to create inflatable pouch actuators that can create linear or rotational motion [79]. PDMS is a silicone-based organic polymer that can be used to fabricate microscale actuators [80]. Smart material composites such as Nitinol, which is a shape memory metal alloy, have very elastic characteristics and can create discrete levels of stiffness [81].

The construction and materials of soft robots are summarized in Table 2.1.

Table 2.1: The construction and materials of soft robots.

Material/Construction	**Purpose - Actuators**	**Benefits**	**Drawbacks**
Silicone [28], [52]–[63]	Pneumatic actuators, Robotic grippers, and Buckling linear actuators	Compliance, versatility, and low cost	Short lifespan and buckling
3D printed materials [22], [50], [64]–[70]	Pneumatic and fluidic actuators	Various 3D printing methods, a high degree of freedom, and low cost	Low tensile strength

Hydrogels [71]–[75]	Bending and fluidic actuators	Easily customizable, many DOF, and small scale	Expensive, low tensile strength, and difficult to handle
Electroactive polymers [76]–[81]	Continuum arms	Large compliance, various stiffness levels, and many DOF	High input voltage/temperature and slow response and recovery times

2.2 Soft Robot Sensing

Since soft robots have the potential to mimic organisms and interface to human bodies, there is an increasing trend towards the development of biomimetic robotic grippers and prosthesis [8], [10]–[17]. Though these designs have exceptional grasp capabilities, most soft robots have limited dexterity and sensing capabilities. Sensors incorporated into soft robots prioritize flexibility and simple fabrication to minimize its effect on the actuation of the soft robots [79], [82]–[88]. Soft robot sensing is usually focused on either tactile sensing or curvature sensing. The sensing modality used by these sensors ranges from piezoresistive, magnetic, and optical. The following sections discuss each of these modalities.

2.2.1 Piezoresistive

Piezoresistive sensors exhibit a change in resistance when a force is applied. The sensors in soft robots are generally composed of composite materials such as polylactic acid-graphene (PLA-G) in thermoplastic polyurethane (TPU) or carbon black in an elastomer/fabric [63], [89], [90]. They can be 3D printed using FDM, can have a high sensitivity, and wide sensing range but can suffer from a high degree of hysteresis [89], [90]. These sensors are generally used for tactile sensing.

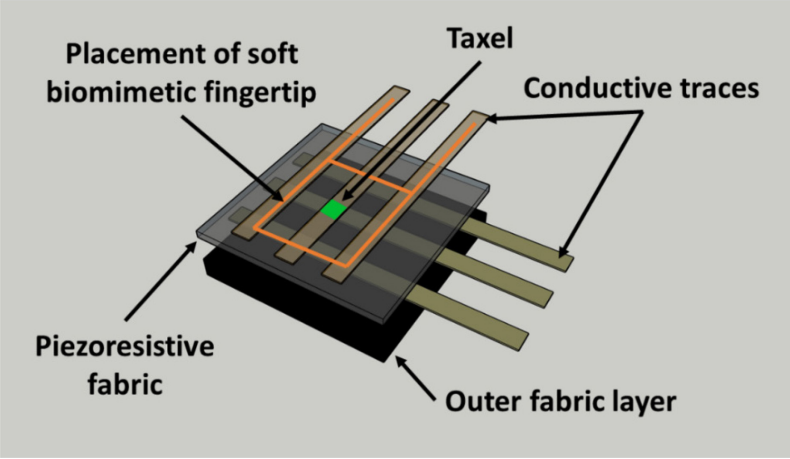

Figure 2.5: Fabric-based piezoresistive tactile sensor [63].

Liquid metal embedded elastomers (LMEE) are elastomers with channels filled with a liquid metal that changes in resistance depending on the degree of deformation or stretch [91]. LMEEEs function as strain gauges but have significantly higher flexibility without fracturing. This allows them to actuate at the same level as the soft robot. Additionally, the microchannels can be laser engraved to create smaller and more precise channels.

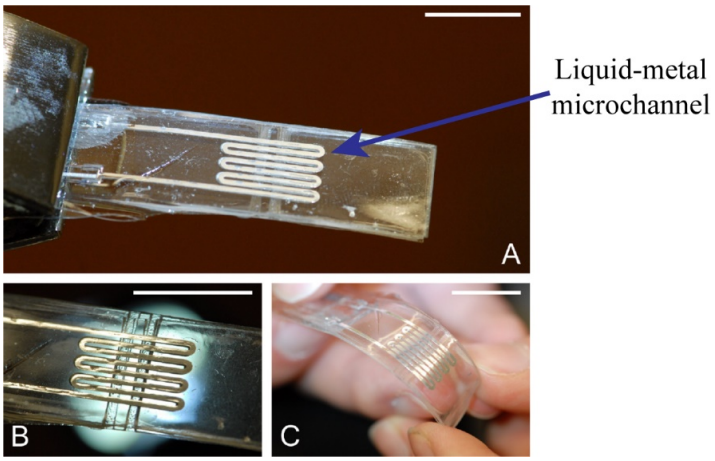

Figure 2.6: Overview of a liquid metal embedded elastomer (LMEE) sensor that can be used to measure the curvature of a soft robot [91].

Semi-conductive polymers consist of conductive particles in a semiconductive matrix that decreases in resistance when there is curvature or force is applied. Therefore, they can be used to fabricate curvature and tactile sensors. These sensors can be fabricated using hydrogels, doping silicone with carbon powder, or 3D printing [56], [92]–[94]. The reliability of the sensor is highly dependent on the homogeneity of the carbon to silicone blend, while the ratio of the material determines the sensitivity and hysteresis [92].

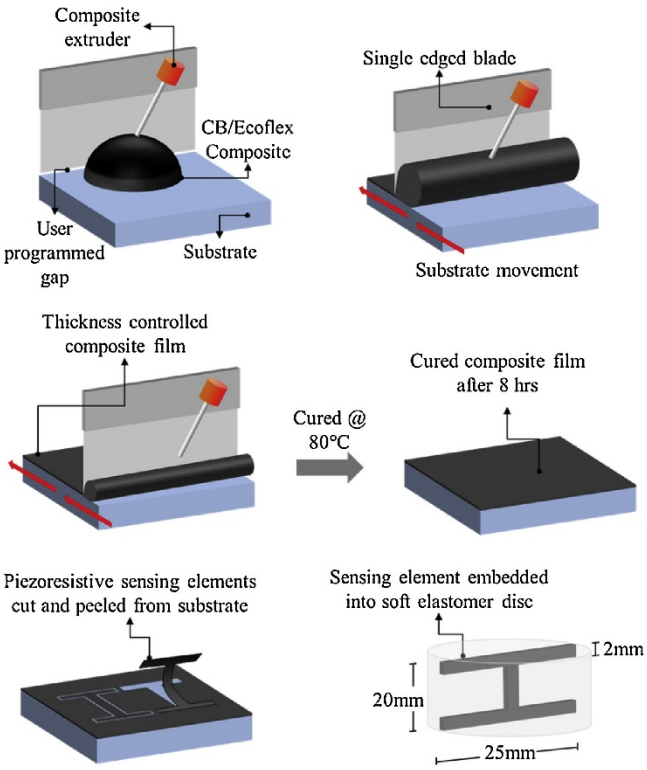

Figure 2.7: Schematic representation of the sensor with Carbon black doped silicone [90].

2.2.2 Magnetic

Hall Effect sensors measure the magnitude of a magnetic field. When a hall effect sensor is combined with an embedded magnet, accurate and rapid tactile and curvature sensing can occur. Additionally, they can have a high sensitivity reaching up to 75 Hz and a low degree of hysteresis [95]. These sensors have been embedded in a silicone mold to measure contact forces for object manipulation [95]–[97].

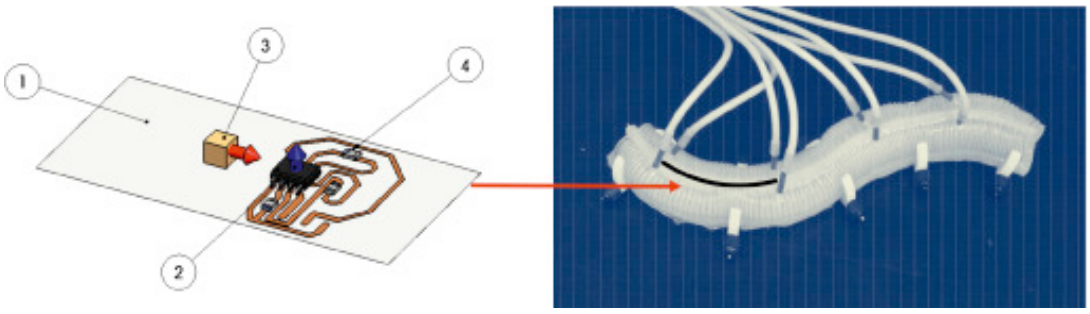

Figure 2.8: Hall effect sensor with a magnet on a soft snake robot for sensing curvature [95]. (1) flexible substrate; (2) Hall effect IC; (3) magnet; (4) circuit paths and components.

2.2.3 Optical

Fiber optic cables have been embedded within soft robots to measure the bending and stretching of the soft robot [13], [98]–[100]. These sensors use a fiber Bragg grating coating that reflects only particular wavelengths of light. Unlike electromagnetic sensors, these sensors are resistant to external interference. Additionally, the fiber optic cables are flexible and do not interfere with the soft robot [98]. However, image processing is required for tactile sensing.

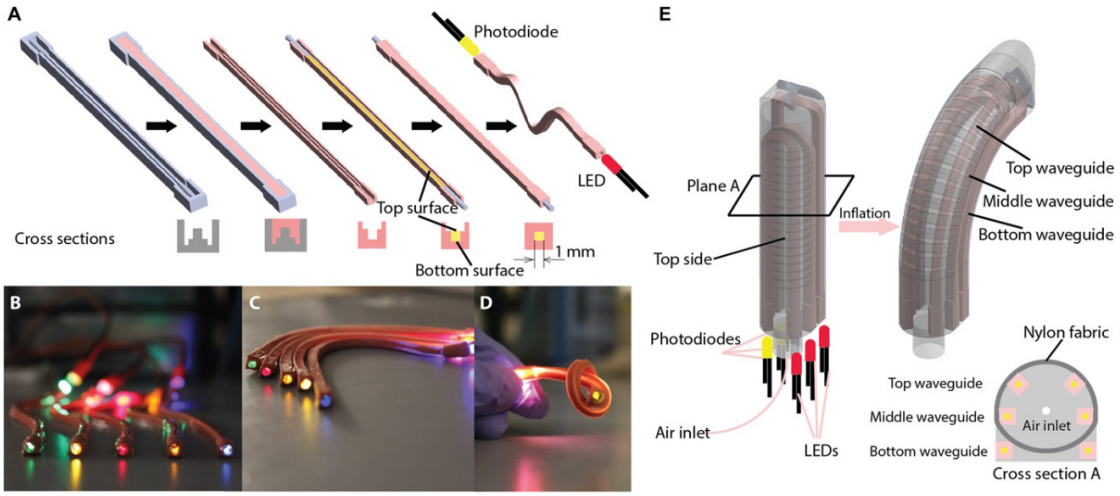

Figure 2.9: Stretchable optical waveguides in a soft robot to sense curvature and force [13].

Table 2.2: Summary of Sensing in soft robots.

Sensing Modality	Material/Construction	Purpose	Description
Piezoresistive	Composite [63], [89], [90]	Tactile	3D printable, a high sensitivity, and wide sensing range; Can have high hysteresis
	Liquid metal [91]	Strain and curvature	Microchannel scale and linearity
	Conductive hydrogel [56], [92]–[94]	Curvature and tactile	Can be constructed with various materials; Reliability depends on the blend
Magnetic	Magnets and hall sensors [95]–[97]	Curvature or tactile	High sensitivity, rapid sensing, repeatable, and low hysteresis
Optical	Fiber optic cables [13], [98]–[100]	Curvature or tactile	Resistant to external interference and repeatable; tactile requires image processing

Chapter 3

Review of Texture Recognition in Prosthesis

The natural sensory feedback loop is an intuitive process for healthy individuals. As afferent fibers are stimulated in response to grasping objects or through dexterous movements, an efferent motor response is used to adjust hand movements as needed. Amputees with conventional prostheses lose the ability to feel when or how an object is being grasped and thus cannot adequately modulate their prosthetic hand movements based on natural sensory stimulation. Replacement of this crucial loop starts with sensors that can detect various stimuli from the surrounding environment and the physical world. Object stiffness and texture can be used to improve the breadth of sensations replaced for amputees while improving grasping tasks. Upon receiving static and dynamic sensory cues, the user can understand and dynamically interact with their surroundings.

Static cues can be obtained instantaneously and a few studies have incorporated these cues into their soft robots such as temperature, curvature, and force [16], [17], [22], [23]. Processing dynamic cues such as texture is more complex as it requires temporal information. As tactile sensing has been shown to help prosthesis users with handling everyday objects, studies have been exploring how to best mimic and replace subdermal receptors for improved grasping control in prosthesis [26], [27]. Many of the currently available texture sensing technologies for prosthesis and their performances at detecting a variety of surfaces are discussed in the following sections. Certain sections are taken from a review that was submitted to Annals in Biomedical Engineering, 2020 [101].

3.1 Biological Tactile Sensing

The design of many prosthetic sensors has been directly inspired by the biological components that are aimed to be replaced. Prosthetic sensors should also mimic the biological characteristics of the skin, including signaling mechanisms [102]–[105], structure [38], and mechanical properties [103], [106], [107]. The human glabrous dermis layer contains four types of low threshold mechanoreceptors (LTMRs), categorized into slow-adapting (SA) and fast-adapting (FA), that measure mechanical stimuli, Shown in Figure 3.1. Among the four LTMRs, Merkel cells (SA1) and Ruffini endings (SA2) produce sustained signals throughout mechanical stimulation. This allows these receptors to measure static force and strain from prolonged contact. Meissner corpuscles (FA1) and Pacinian's corpuscles (FA2) produce dynamic signals and are more involved in the detection of features of an object and vibration [108].

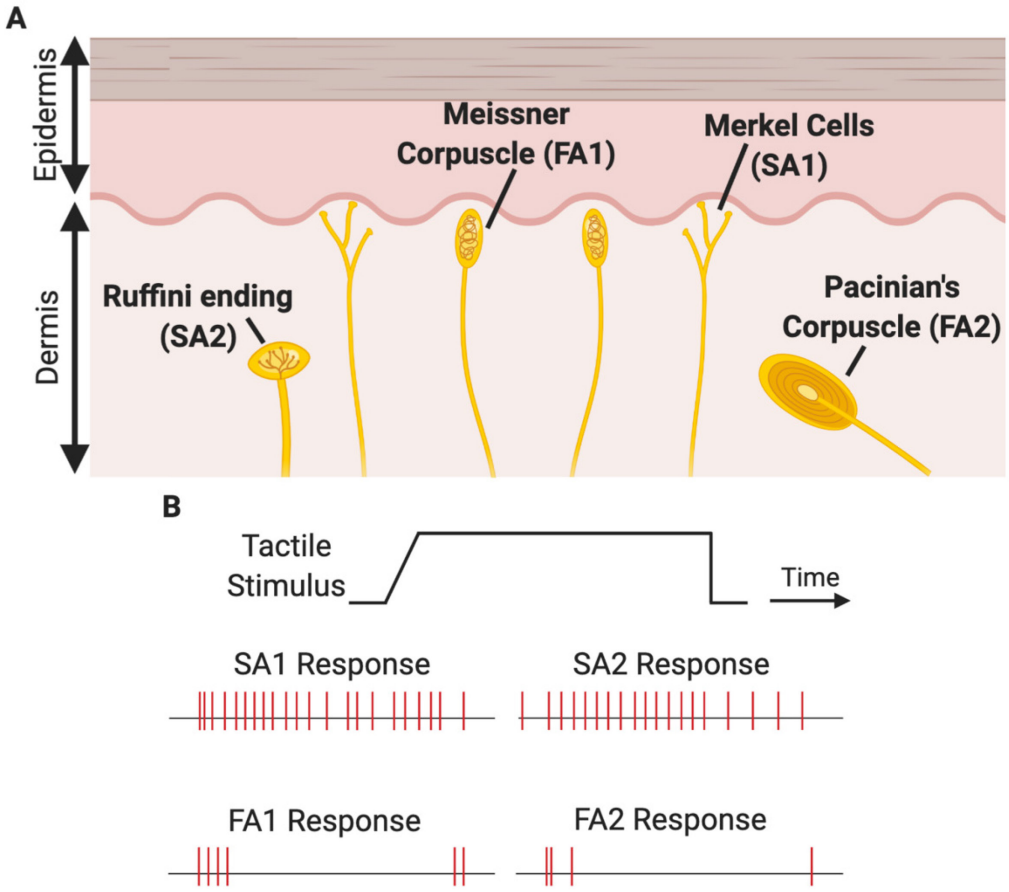

Figure 3.1: Schematics of human glabrous skin mechanoreceptors and firing patterns. **(A)** Glabrous skin contains four types of LTMRs: FA1, FA2, SA1, and SA2. **(B)** In response to a tactile stimulus, the four LTMRs show different firing patterns.

3.2 Prosthetic Tactile Sensing

Prosthetic sensors are used to detect external stimuli such as force and pressure at the fingertips of a prosthesis. Common electronic components that detect force and transduce the information directly to electrical signals are the most apparent and available solutions. These synthetic sensors are often adapted and modified to allow for more specificity and sensitivity at the range that would be common for human interaction.

Custom sensors that are designed based on biological components of the hand are referred to as biomimetic sensors.

3.2.1 Synthetic Sensors

Synthetic sensors detect contact forces by measuring internal changes in resistance, capacitance, or inductance due to an externally applied force. The sensitivity and working range of these sensors can depend on which method of measuring the applied force is used. However, the working range can be improved by modifying the contact surface with more compressive materials such as synthetic polymers. While synthetic sensors aim to replace lost sensory information, the design strategy is not inspired by the lost biological skin or afferent fibers. Instead, this group of sensors leverages the availability and functionality of common electrical components that are manufactured on an industrial scale.

3.2.1.1 Resistive Sensors

Resistive sensors are commonly used in tactile sensors for texture detection [35], [36], [38], [102], [109]–[114]. Micro-electromechanical systems (MEMS) have wide applications for creating highly sensitive tactile sensors that convert mechanical deformations into electrical resistance through multi-axial piezoresistive sensors. The deflection of these resistors, when scanning over surfaces, can define micro-structural differences as the sensor moves across the surface that is indicative of specific texture features. This method can detect pressure changes of fine weave patterns of paper textures [34], [110]. Other MEMS-based capacitance sensors with a linear array of four tactile sensors were able to detect surface patterns as small as 200 μm and could obtain characteristic frequencies that encode texture differences between smooth PDMS surfaces

and nylon. Distinct characteristic signals could be detected for each texture after the multi-array sensor signals were fast Fourier transformed, exhibiting the capability of multi-array sensor configuration to capture both temporal and spatial information. This would enhance the potential for texture pattern detection significantly [41].

Novel fingerprint-inspired single-walled nanotube (SWNTs) and PDMS composite piezoresistive sensors are flexible, able to discern a useful range of pressures during scanning movements (45–550 Pa), and can detect changes in resistance from 0–2,500 Pa. A double-sided, double-layered, interlocked pyramidal SWNT micro-structures can detect even minute changes in shear force. Even fine periodic texture patterns with 15 μm interval spacings were detected with discernable output signal changes. This feat highlights the SWNT's high recovery rate after shear force, attributed to the pyramidal microstructure design. Minute differences in various fabric textures could easily be identified based on their output signals [38].

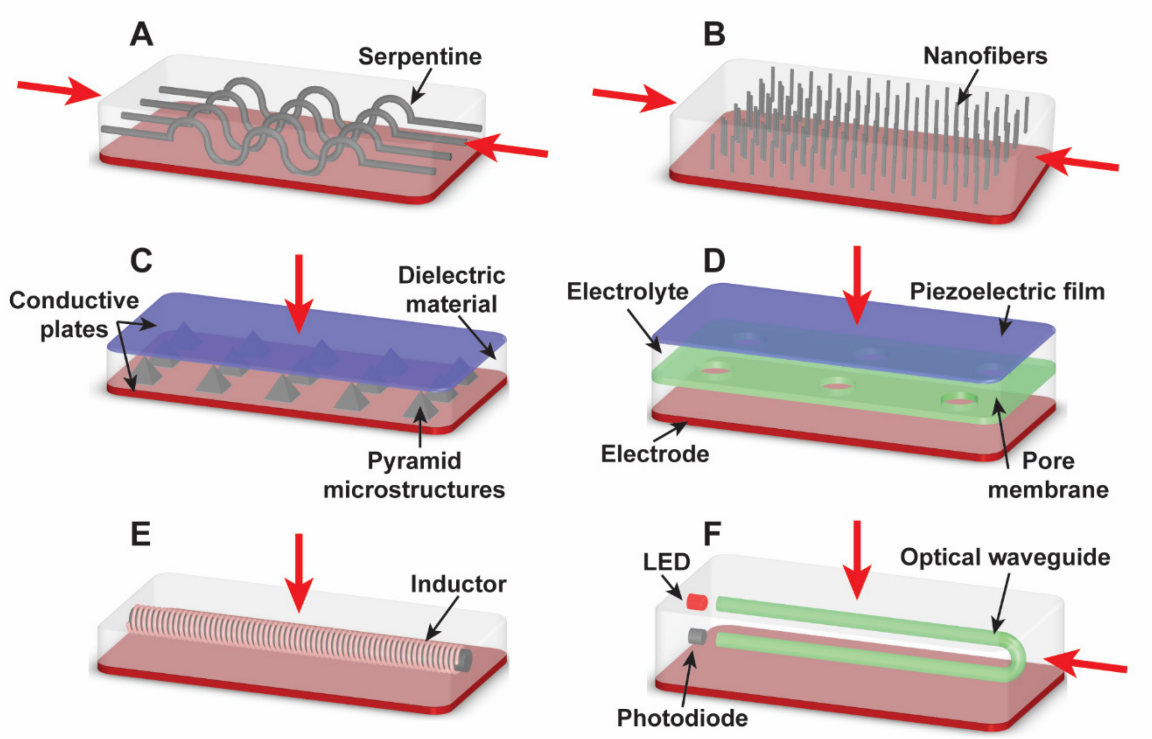

Figure 3.2: Representations of the different synthetic sensors: (A) serpentine and (B) nanofiber elements of strain gauges in resistive sensors [115], (C) pyramid microstructures in the PDMS layer to create a more sensitive capacitive sensor [116], (D) pore membrane in a piezoelectric sensor to create artificial ion channels [104], (E) inductor in an inductive sensor to create digital-frequency signals [117], (F) optical waveguides in optical sensors that can be embedded in prosthesis [118]. Red arrows indicate the directions of deformation that the sensors detect.

A composite of graphene flakes and polyurethane sponges have been integrated for use as an improved conductive graphene piezoresistive sensor [35]. However, the sponge material is slow to return to its original shape after deformation. Despite this extended time dependency, the signal acquisition still maintained low enough noise artifacts versus the actual signal to distinguish characteristic FFT peaks. The graphene composite allowed for distinguishable FFT characteristic signals for ridge (grooved surface structures) detection with a minimum of 200 μm separation on fabricated PET material [36].

3.2.1.2 Piezoelectric Sensors

Piezoelectric (PE) sensors measure applied force and strain by generating a voltage difference. PE sensors using PVDF have exhibited sensitivity to external input that produces distinguishable voltage signals [39], [112], [113], [119]. One of the main characteristics of PVDF is the ability to mix other chemical compounds into the structure of PVDF. The introduction of impurities dictates the "roughness" of the PVDF film and determines the piezoelectric sensitivity to external surfaces. A PVDF film was used to determine the differences in different weave fabrics. Detection and classification of different surface types were done by extracting features from the output frequency and classified through an unsupervised k-means clustering algorithm [39].

Flexible two-layered PVDF sensors showed enhanced sensitivity and higher resolution (0.43 μm), with capabilities to differentiate between texture signals of polished metal surfaces. The perpendicular orientation of the two PVDF films allowed for increased signal acquisition and the ability to sense vibrational differences between the two sensors during scanning. Despite the higher sensitivity PVDF sensor arrangement and the use of various machine learning algorithms, the accuracy of classifying polished metal surfaces was much lower than that of fabric detection [39]. This could be attributed to the increased innate difficulty of sensing the minute sandpaper gratings between polished metals, which would even prove to be challenging for a human fingertip [31], [32].

3.2.1.3 Capacitive Sensors

Capacitive sensors that measure changes in capacitive coupling across materials have been used in designs that allow for pressure detection, shear force sensing, and texture

recognition [41], [120]. Polymers such as PDMS have been used in mesa micro-structures to achieve flexible and sensitive sensors [116], [121], [122]. To increase capacitance sensitivity, the PDMS dielectric layer can incorporate different micro-structures such as pyramids and v-shaped grooves (Figure 3.2). Certain capacitive sensors measure applied force on the capacitive plates due to geometric changes in the capacitor [107], [123], [124]. MEMS-based capacitance sensors with a linear array of four tactile sensors were able to detect surface patterns as small as 200 μm and could obtain characteristic frequencies that encode texture differences between smooth PDMS surfaces and nylon. Distinct characteristic signals could be detected for each texture after the multi-array sensor signals were fast Fourier transformed, exhibiting the capability of multi-array sensor configuration to capture both temporal and spatial information. This would enhance the potential for texture pattern detection significantly [41].

3.2.2 Biomimetic Sensors

Piezoresistive sensors have been used in the design of organic prosthetic sensors that mimic the biological signaling activity of SA and or FA mechanoreceptors, forming a digital mechanoreceptor. The transduction from analog sensor reading to spiking signals was achieved either through an electronic circuit or a software model. An oscillating circuit that produced a periodic square wave was used to encode physical force stimuli into digital signals [102]. Pyramidal micro-structures were constructed from polyurethane elastomers with embedded carbon nano-tubules. This combination of piezoresistive sensors and organic oscillators enabled varying sensor output frequencies, which mimicked SA

mechanoreceptors. Increased sensitivity and working range of the sensor was achieved by reducing the effective Young's modulus and concentrating the electric field.

Another sensor that was designed to mimicked the SA signaling mechanism uses conductive micro fluids encapsulated in polymer film to form a hemisphere [103]. The volume of fluid and diameter of the hemisphere could be adjusted to control the sensitivity of this fluid-based resistive sensor. Normal forces and shear forces were detected by measuring the concurrent resistance changes, which showed a similar profile to SA skin receptors. The activity of FA receptors has been reproduced by a sensor design that used PVDF as the conductive piezoelectric material and PDMS as the coating [104]. Continuous electrical signals were converted into spike trains with variable frequency, based on a neuron model that describes the current change across FA mechanoreceptors. This conversion from the voltage output of the sensor to a spike train mimicked the FA receptor response (Figure 3.3).

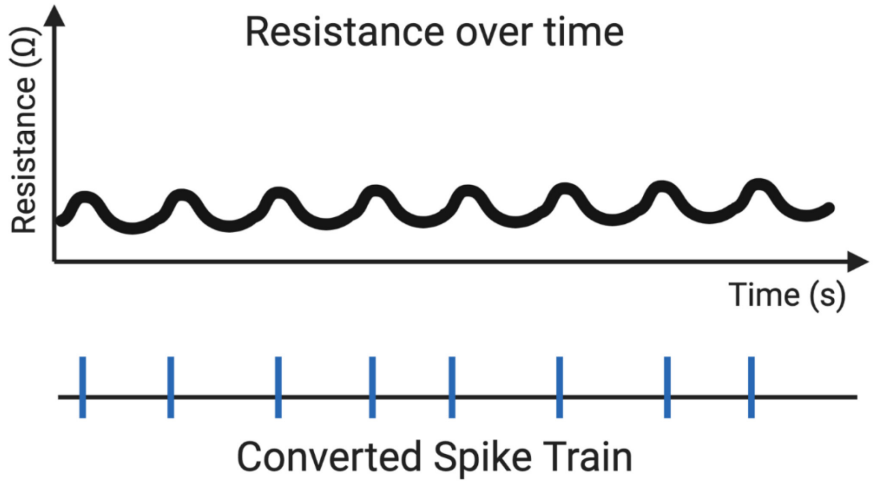

Figure 3.3: Analog changes in resistance of a sensor are converted to a digital spike train, which is similar to the firing pattern of FA mechanoreceptors.

More recently in 2018, a self-powered piezoelectric sensor achieved properties of both SA and FA mechanoreceptors. To realize both SA and FA responses, this sensor needs to generate two types of voltage outputs, one corresponding to SA and the other FA, in response to pressure [105]. The sensor consists of a piezoelectric film made with gold and PVDF as well as an artificial ion channel made with an electrolyte (PANI solution) and a pore membrane. Applied pressure to the sensor deforms the piezoelectric film, allowing for the encoding of an FA response. As contact is maintained, ion movement through the electrolyte in the membrane occurs, creating a sustained SA response. The sensor was demonstrated to identify mechanical stress and detect grasping events such as slipping objects.

Prosthetic sensors have also been designed based on the surface structure of fingerprints. A flexible tactile sensor has been developed with microscale pyramids on both the outer layer in contact with the object surface and between the inner layers of the sensing element (Figure 3.4) [38]. This sensor, with the outer pyramid layer inspired by shaped grooves of fingerprints, was made of single-walled carbon nanotubes (SWNTs), polyethylene, and PDMS. Two inner layers of SWNT formed pyramids that were organized into an interlocked layout, allowing for the sensor to detect changes in both normal and shear forces. The use of pyramidal structures allowed for high sensitivity, as the tip of the pyramid deforms more easily upon applied force than a smooth surface with more direct contact and rigidity.

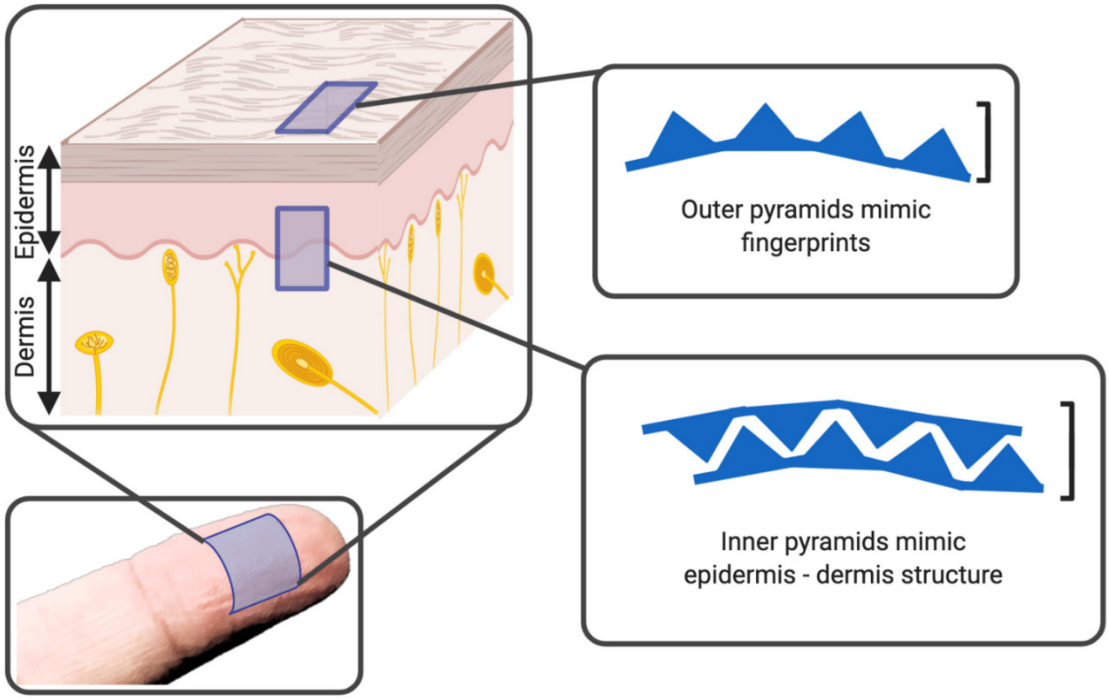

Figure 3.4: Structural layout of sensors (right) that mimic different parts of the skin. Outer pyramids mimic grooves on the skin surface and interlocking pyramids mimic the connection between the epidermis and dermis.

Biomimetic sensors have also sought to copy the compressive nature of skin along with its ability to stretch. Most tactile sensors described so far have used stretchable materials such as elastomers to mimic basic viscoelastic properties of the skin surface. However, the sensing elements themselves were underneath this skin layer. Flexible sensors can be manufactured to accommodate skin-like mechanical properties across the sensor itself. Silicon-based circuits can be pre-strained to provide sustained force detection in thin, deformable layers while under strain due to applied forces [125]. The same pre-straining strategy was applied to develop a skin-mimicking, stretchable sensor using silicon nano-ribbons covering an entire artificial hand. The local curvature of the ribbon is site-specific and can be calibrated to conform with the curvatures of the prosthetic hand, thus

corresponding to the natural elasticity of the hand region. A greater curvature corresponds to heightened elasticity and lowers piezoresistive sensitivity [106].

The extent of biomimicry in prosthetics is not limited to mechanical properties and sensory end organs. The premise of wound healing has also been explored in terms of prosthesis healing. Made of a dynamic, covalent thermoset doped with silver nanoparticles, a re-healable sensor was able to reform its original structure after external damage due to an abrasive cut. Application of a polymerization compound solution and heat allowed for covalent bond exchange reactions at the wound site, enabling the healing of the sensor surface [107]. Although the capacitance profile of the original, undamaged sensor was not completely retained after the healing process, it did allow for similar object detection.

The performance of tactile sensors and their different texture recognition techniques are summarized in Table 3.1.

Table 3.1: Comparison of texture recognition techniques in recent works.

Ref.	Materials	Textures	Methods- Algorithms	Accuracy
[30], [32]	2-layer PVDF	8 graded ridged textures	Discrete wavelet transform (DWT), kNN, SVM, ELM, VPd, van Rossum distance	80–97%
[31]	2-layer PVDF	15 graded polished metals	kNN, SVM, ELM	57–73%

[37]	Silicon MEMS	10 natural textures of which 5 are fabric	Izhikevich neuron model, kNN, VPd	68% - 97%
[33]	Acrylic MEMS	10 graded textures	Izhikevich neuron model, ELM, mechano-neuro-transduction	92%
[34]	Silicon MEMS	5 artificial Texture patterns	Maximum Likelihood	53–61%
[35], [36]	Graphene Sponge	2 PET gratings	FFT	NA
[38]	SWNTs/ PDMS	2 Silk fabrics, and 5 Braille letters	FFT	NA
[39]	PVDF	5 types of fabrics including silk, cotton, and wool	RBF, k-means clustering	96–100%
[40]	Multi-strain gauge, PVDF	8 surfaces: carpets (2), sponge, tiles (2), vinyl, wood, fabric	Decision Trees (Naïve Bayes, boosted tree)	80–100%

[41]	Silicon MEMS	3 - Smooth PDMS surface, polycotton, nylon	FFT	NA

Chapter 4

Texture Discrimination with a Soft Biomimetic Finger using a Flexible Neuromorphic Tactile Sensor Array that Provides Sensory Feedback

The following chapter was submitted as part of a journal article to Soft Robotics and has been recently accepted in August 2020 [126].

4.1 Design and Fabrication

4.1.1 Sensor Array Design

Sensors incorporated into soft robots prioritize flexibility and simple fabrication to minimize its effect on the robot's actuation. The design of the flexible, textile tactile sensor array (Figure 4.1) was inspired by the mechanoreceptors found in the epidermis of the

human body [127]. This variation of a piezoresistive tactile sensor was easily integrated with the fingertip of the soft biomimetic finger, which was fabricated mainly from silicone and fabric. Additionally, the sensor does not interfere with the normal actuation of the soft biomimetic finger. The 3x3 tactile sensor array has 9 taxels, or sensing elements, to convey spatial information about the textures. This type of sensor can be easily scaled to cover a larger surface area with more taxels to provide additional spatial information.

The tactile sensor was fabricated using conductive fabric traces (LessEMF, Latham, NY) and piezoresistive fabric (Eonyx, Pinole, CA), which transforms the force applied on the material into changes in resistance. The piezoresistive fabric is sandwiched between 2mm perpendicular crossing strips of conductive fabric. This creates a 2x2 mm^2 sensing surface area for each taxel. The conductive fabric traces are spaced 2.5 mm apart. A black, protective, elastic fabric encases the entire sensor array. Due to these low-cost materials, the textile tactile sensor benefits from a low manufacturing cost.

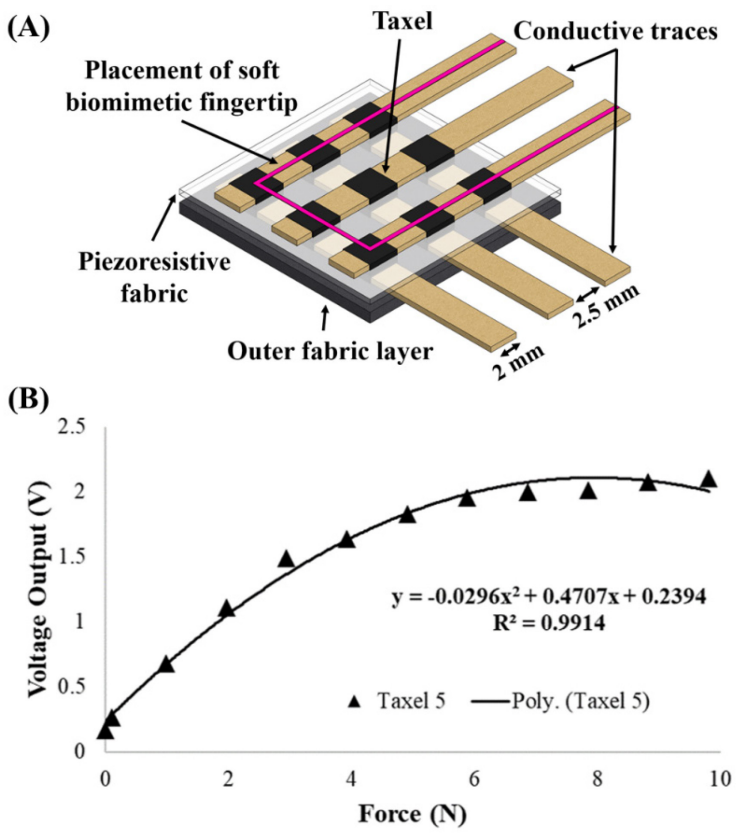

Figure 4.1: (A) Graphic of the flexible textile tactile sensor array. The 3x3 sensor array has 9 4 mm^2 taxels (or sensing elements) spaced 2.5 mm apart. The tactile sensor array is integrated at the fingertip of the soft biomimetic finger. **(B)** The characterization curve of the tactile sensor (Force vs Voltage response) was created by placing 11 calibration weights, ranging from 10g to 1000g, onto the taxel using an end effector tip. Each weight was applied once per taxel. The characterization curve of the center taxel, taxel 5, is shown as it makes the most direct contact with the textures. The other taxels follow a similar curve with a consistent range of linear response.

The voltage response of the tactile sensor array was measured using an Arduino Mega 2560 microcontroller. Each common line of the sensor was connected in series with a 10 kΩ resistor, acting as a voltage divider. For this study, the exact value of the applied force is not necessary, as the texture discrimination method with neuromorphic encoding uses the relative forces measured across the textures.

4.1.2 Soft Biomimetic Finger Design

The pneumatically actuated soft biomimetic finger has three joints with two independently controllable degrees of freedom, similar to a human finger (Figure 4.2). It was fabricated from Dragon Skin™ 10 Medium (Smooth-on, Macungie, PA, USA) silicone rubber and two inextensible materials, cotton fiber and cotton fabric.[28] The fracture strength for the silicone rubber, which is the measure of the material's ability to resist failure during elongation, is 1000%. Dragon Skin™ rubbers have previously been used for applications from medical prosthetics to special skin effects [9], [128], [129]. Since the soft biomimetic finger was constructed from silicone and fabric, it has a low manufacturing cost and is very compliant.

Using the concept of hybrid fiber-reinforced actuators, the two inextensible materials behave as strain-limiting layers to reinforce the actuator and prevent radial expansion [130]. To create the air channels in the actuator, the silicone prepolymer was poured over carbon fiber rods, separated by a block of silicone, during the fabrication process. The carbon fiber rods serve as the template for the air cavity and the block of silicone separates the two air channels. Next, two layers of cotton fiber (0.1 mm thickness) were wound around the cured silicone inner bladder with a pitch of 0.4 mm to completely cover the inner bladders. Next, three strips of cotton fabric, one 20 mm and two 8 mm width strips, with a length of 96 mm were applied at specific intervals along the soft finger. The 20 mm strip was applied around the section of silicone between the two pneumatic channels to mimic the proximal phalange. The 8 mm strips were applied on the soft biomimetic finger at specific intervals to mimic the distal and intermediate phalanges of a

human finger. The sections of silicone not wrapped with these fabric strips are intended to create the metacarpophalangeal (MCP), proximal interphalangeal (PIP), and distal interphalangeal (DIP) joints (Figure 4.2). The fiber and fabric-reinforced inner section was then coated with a final layer of silicone. To seal the fingertip, a small silicone rod and silicone glue were added to the distal end of the soft finger. Finally, a strip of fabric, 100 mm by 12 mm, was adhered to the palmar surface of the soft finger. This final strain-limiting layer of fabric creates the directional curvature that mimics the human finger. Through this process, the pneumatically actuated soft biomimetic finger's three joints with two degrees of freedom were created.

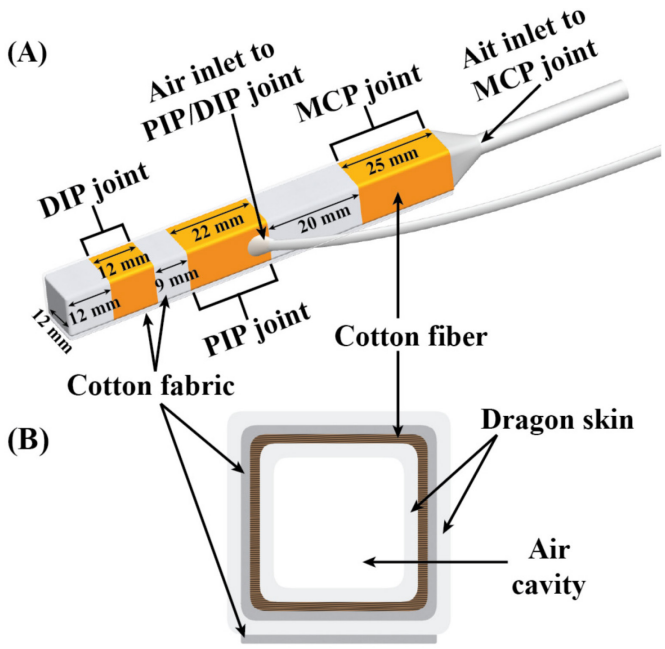

Figure 4.2: (A) Isometric view of the soft biomimetic finger model. (B) Graphical cross-section of the soft finger.

The angle of flexion of the soft biomimetic finger is determined by the actuation pressure, with a linear relationship during the simultaneous actuation of both air channels

(Figure 4.3). The pneumatic setup (Figure 4.3C) used an air compressor and two 3-way direct-acting solenoid valves to regulate the airflow into the soft biomimetic finger. Each valve is connected to an air channel's inlet and a pressure sensor (Honeywell ASDXACX100PAAA5). The pneumatic circuit is independently controlled by an Arduino microcontroller.

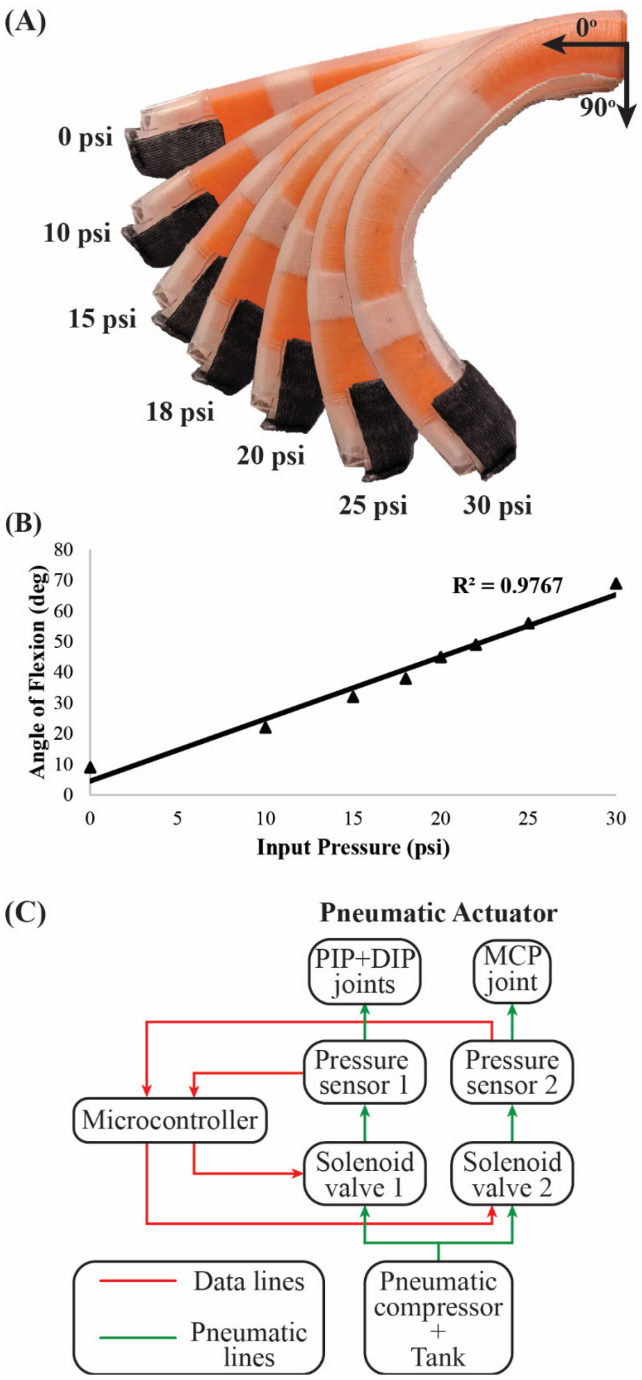

Figure 4.3: (A) Side view of the simultaneous actuation of both joints at varying pressures when mounted horizontally on the UR5 robot arm. **(B)** The angle of flexion of the soft biomimetic finger in response to the pneumatic actuation pressure. The angle of flexion is the degree to which the fingertip moved when the soft finger flexed during actuation compared to the 0° horizontal reference at the base of the soft finger. **(C)** Overview of the pneumatic setup used to actuate the soft finger.

4.1.3 Textured Plates Design

A total of 13 textured plates were designed and 3D printed out of Polylactic acid (PLA) to assess the soft finger's texture discrimination capability (Figure 4.4). These 108x36 mm^2 textured plates, with varying texture elements, were passively palpated by the soft biomimetic finger. The varied texture elements of the textured plates require both spatial and temporal information to accurately discriminate between the textures. The 36x36 mm^2 textured surface was centered along the plate to create an isolated surface for palpation. Each texture was raised 2.5 mm above the top plane of the textured plate.

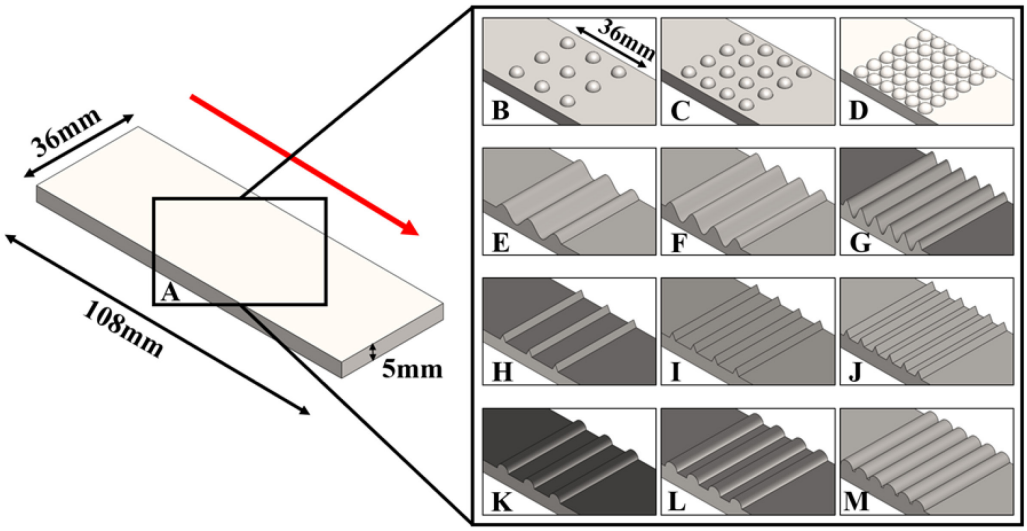

Figure 4.4: Textured plates designed to test the soft biomimetic finger's ability to discriminate textures. The four main texture elements are hemispheres (B-D), sinusoidal waves (E-G), triangular ridges (H-J), and curved ridges (K-M). These texture elements were varied by 3, 4, or 6 rows and combined with the flat (A) texture created 13 total textured plates. The red arrow indicates the direction of palpation.

4.2 Methods

To test texture discrimination in this study (Figure 1.1), the soft finger passively palpated the 13 textured plates at four speeds and four actuated states. This resulted in 16 total parameters being tested over the 13 textured plates to determine the texture discrimination ability of the soft finger at varying conditions.

4.2.1 Experimental Procedure

Consistent palpation of the textures required a robust testing method with a gripper that held the soft biomimetic finger without inhibiting its actuation. Thus, the soft finger's MCP inlet was held by the gripper to allow normal actuation and was mounted to a UR5 Robot arm (Universal Robots, Odense, Denmark) to palpate the textured plates. First, the soft biomimetic finger was brought down onto one side of the textured plate until the fingertip was between 10º to 15º compared to the textured plate and applied a normal force of 1 N (Figure 4.5). The soft finger was held at this angle to achieve maximum surface contact of the sensor onto the texture. Then, the soft finger palpated the textured plates by being moved along the direction shown in Figure 4.4. Finally, the soft finger was moved back up and to the start position. A complete loop of the UR5 robot arm was considered one trial. Each of the 13 textures was palpated with 80 trials for all 16 parameters. The voltage response of each taxel was sampled by the Arduino Mega 2560 microcontroller at 100 Hz and processed in MATLAB.

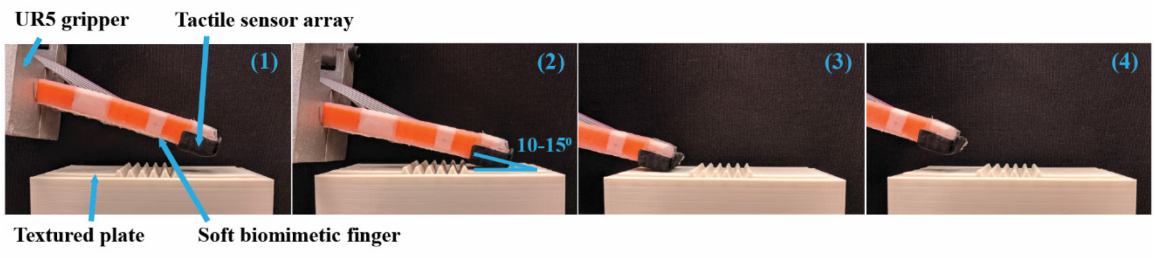

Figure 4.5: Overview of the different positions of the soft biomimetic finger in a trial with the positions numbered in chronological order. The soft finger was mounted on the UR5 robot arm and is shown during passive palpation of textured plate G, while at 0 psi. The soft finger was held at 10 - 15º compared to the textured plate. In position (2), the soft biomimetic finger is brought down until it applies 1 N of force, measured on taxel 5.

To comprehensively test the texture discrimination capability of the soft biomimetic finger at different conditions, tests occurred at varying speeds of palpation and levels of actuation. To test the ability of the soft finger at varying speeds of palpation, the UR5 robot arm moved the soft finger at 23 mm/s, 44 mm/s, 64 mm/s, and 81 mm/s. The soft finger was also tested at varying pressure levels for simultaneous joint actuation: 0 psi, 10 psi, 15 psi, and 18 psi. This changed the duration of each trial for the 16 parameters, which is shown in Table 4.1. Though the soft biomimetic finger could actuate up to 30 psi and create a larger bending angle, this was not feasible in this testing environment. Beyond 18 psi, proper contact of the fingertip to the textures on the plates was not achievable.

Table 4.1. Duration of a single trial for each parameter.

		Palpation Speed (mm/s)			
Actuated Pressure (psi)		23	44	64	81
	0	9.8 s	5.65 s	4.27 s	3.57 s
	10	10.62 s	6.06 s	4.54 s	3.78 s
	15	11.54 s	6.52 s	4.84 s	4.01 s
	18	12.15 s	6.82 s	5.05 s	4.16 s

4.2.2 Neuromorphic Encoding

Neuromorphic encoding was used due to its computational efficiency in encoding information and its biological relevance for afferent nerve stimulation [33], [131], [132]. The encoding of spatial and temporal information is important when processing dynamic cues such as texture. The Izhikevich neuron model was used to mimic the mechanoreceptor activity of the tactile epithelial cells called Merkel cells [133]. To utilize the Izhikevich framework, the tactile response from each taxel was converted using the tonic spiking model. This model exhibits a steady-state spiking pattern after the initial onset and is used as the basis for the slowly adapting (SA-1) neuron spiking patterns (Figure 4.6). This neuromorphic encoding method has been used previously for similar applications [29], [33], [44], [46]. The Izhikevich neuron model uses equations (4.1), (4.2), and (4.3) to generate the spike train with injected current *I,* neuronal membrane voltage *v*, and recovery variable *u,* which represents the activation and inactivation of K^+ and Na^+ ionic channels [133].

$$\frac{dv}{dt} = 0.04v^2 + 5v + 140 - u + kI \qquad (4.1)$$

$$\frac{du}{dt} = a(bv - u) \qquad (4.2)$$

$$if\ v \geq 30\ mv, then \begin{cases} v \leftarrow c \\ u \leftarrow u + d \end{cases} \qquad (4.3)$$

The voltage response of each taxel was normalized and a gain factor, *k*, of 75 was applied, which was best for classification. This normalized and amplified signal served

as the input current for the neuron spiking model. The Tonic Spiking model's parameters are a = 0.02, b = 0.2, c = -65, and d = 8.

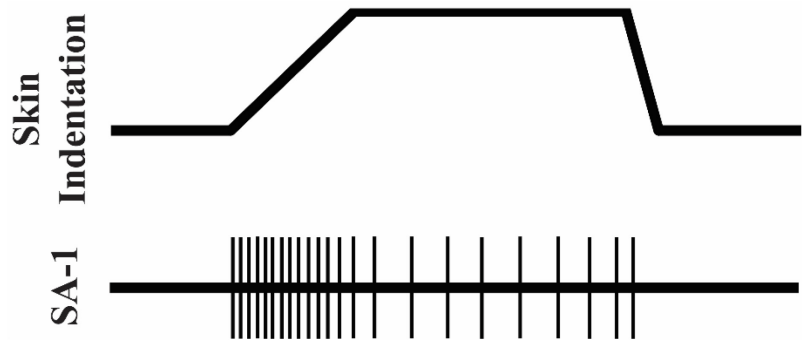

Figure 4.6: Spiking response of a slowly adapting (SA1) neuron in response to a tactile stimulus.

For each texture and testing parameter, the spiking responses from the sensor array were segmented into windows corresponding to the duration of the loop based on each parameter (Table 4.1). These windows were converted offline into spike trains with the Izhikevich neuromorphic model. To compress the information and serve as the features for the classification algorithm, the average inter-spike interval and mean spike rate were calculated for each taxel in every trial window. The average inter-spike interval was calculated by measuring the time elapsed between spikes and averaging those values in each window. The mean spike rate was calculated by tallying the number of spikes in 100 ms bins and dividing it by the bin length, followed by averaging those values in each window.

4.2.3 Classification Algorithms

To test the ability of the soft biomimetic finger to classify textures, the two features from each taxel in a window were used as inputs for SVM's multiclass linear classification model. Specifically, the linear kernel of SVM from MATLAB was used because the assumptions of normal distribution and similar within-class variance were not required. A supervised learning algorithm was chosen because the identities of the textures were known. In our preliminary texture discrimination studies, this classification algorithm has been shown to classify textures well [29], [46].

Eighteen features, 2 per taxel for each trial, from the compressed spiking information were used as the input for the classifier. To reduce the bias of the model, the k-fold cross validation procedure was done using the classical statistical methods [134], [135]. This procedure randomly splits the dataset into k groups. Then, a single group is taken out as the test data set and the remaining groups are used as the training data set. A model is first fit on the training data set and subsequently evaluated on the test data set. Finally, the evaluation score is retained and the same process is completed on the remaining groups. The final classification accuracy is the combination of the result from all groups. In this experiment, a k=4 was used on the 80 trials per texture plate, resulting in splits of 75% training and 25% testing.

4.2.4 Sensory Feedback

Upon classification of the textures, the textural information should then be conveyed to the user. To investigate whether a user would be able to differentiate different textures, transcutaneous electrical nerve stimulation (TENS) was used for sensory

stimulation. This technique has been used previously for conveying touch and pressure information to an amputee [44], [136]. As a demonstration of sensory feedback for textures, four stimulation conditions based on frequency and pulse width were tested. These four stimulation conditions represented a subset of four textures with varied textural information but did not directly correspond to those texture patterns. Three healthy able-bodied subjects participated in this study that was approved by the Johns Hopkins Medicine Institutional Review Board. Sensory mapping was first performed to obtain a stimulation site on the subject's wrist that activated the referred sensation in their hand. During sensory mapping, a beryllium copper (BeCu) probe was connected to the isolated current stimulator (DS3, Digitimer Ltd., UK), which provided a monophasic current. A 5 mm disposable Ag/AgCl electrode (Norotrode 20, Myotronics, USA) was placed on the stimulation site for three psychophysical experiments.

To determine the stimulation frequency that separates discrete and continuous perception of sensation at the referred sensation site in the phantom hand, a discrete vs. continuous frequency detection experiment was conducted [136]. Two frequencies from this experiment were selected and designated as the low frequency (discrete) and high frequency (continuous) conditions. Then, to determine the minimum level of stimulation that is detectable by the subject, a stimulation detection experiment was subsequently conducted [136]. The pulse width of the stimulation was varied while the frequency was held constant at the previous discrete or continuous frequency value. From this experiment, two pulse widths were selected and designated as the low intensity and high-intensity conditions. For each experiment, the subject received 2 seconds of stimulation and verbally

indicated if they perceived the stimulation as discrete or continuous. The data was fitted with a psychometric function using a sigmoid as shown in equation (4.4), where α is the detection threshold and β is the discrimination sensitivity.

$$\frac{1}{1+e^{-(x-\alpha)/\beta}} \qquad (4.4)$$

Finally, a conditional discrimination experiment was conducted to investigate whether the subjects could differentiate one condition from another. The subjects were presented with two 2-second stimulations, with a 1-second interval. The subjects then reported whether they perceived the two stimulations as the same or different. Table 4.2 shows the pulse width and frequency parameters used for the condition discrimination experiment for each subject (AB01, AB02, and AB03).

Table 4.2: Stimulation parameters for the condition discrimination experiment.

		AB01		AB02		AB03	
		PW (ms)	Freq (Hz)	PW (ms)	Freq (Hz)	PW (ms)	Freq (Hz)
Condition	1	1	10	2.5	10	5	5
	2	10	10	10	10	10	5
	3	1	50	2.5	50	5	50
	4	10	50	10	50	10	50

4.3 Results and Discussion

4.3.1 Neuromorphic Encoding

The voltage response from the tactile sensor was converted into spiking patterns by passing it through the neuromorphic model (Figure 4.7). Slowly adapting neurons

primarily respond to the amplitude of the injected current. Therefore, they spike throughout the presence of a texture, following the spatial features of that texture. As such, the spike train generated through passive palpation followed the spatial features of the textures. Due to the compliance of the soft biomimetic finger and flexible tactile sensor, the spatial features of the textured plates were accentuated and provided a distinct and reliable response to each texture.

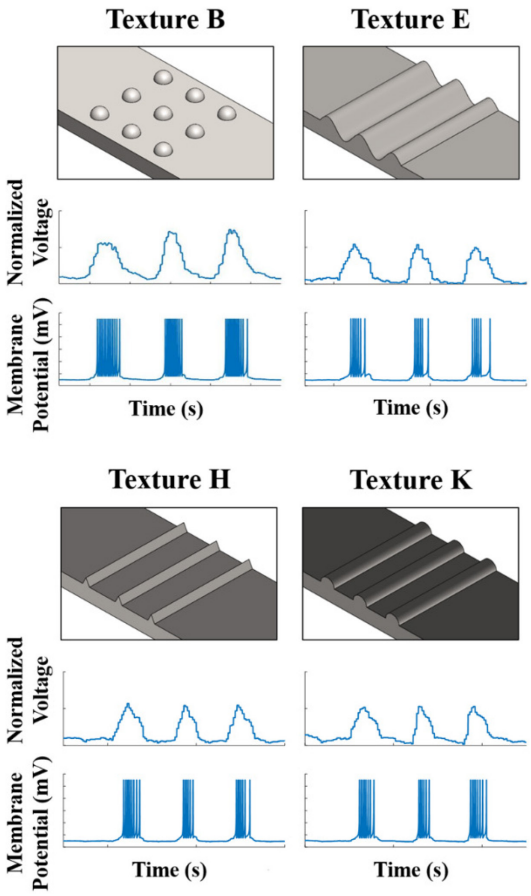

Figure 4.7: Spiking responses from a single taxel on the tactile sensor based on the voltage responses from Textures B, E, H, and K. The spiking responses shown were from the soft biomimetic finger when it palpated the textures at 23 mm/s and was actuated to 15 psi.

4.3.2 Classification Performance

The soft biomimetic finger was tested at 4 speeds of palpation and 4 levels of actuation. The goal was to test the soft biomimetic finger over the 16 parameters to characterize and show how accurately it was able to classify the textures. When run through the pipeline, the soft finger was able to reliably classify all 13 textures at each of the parameters. The overall classification accuracies of each parameter are shown in Table 4.3. The average of the overall classification accuracies for the parameters was 99.57%.

Table 4.3: The overall classification accuracies of the soft biomimetic finger in each parameter.

		Palpation Speed (mm/s)			
		23	**44**	**64**	**81**
Actuated Pressure (psi)	**0**	**98.65%**	**99.52%**	**99.90%**	**99.52%**
	10	**99.33%**	**99.62%**	**99.04%**	**99.81%**
	15	**99.62%**	**99.42%**	**99.42%**	**99.81%**
	18	**99.71%**	**100.00%**	**99.71%**	**100.00%**

The confusion matrix of one parameter, 23 mm/s and 15 psi actuation, is shown (Figure 4.8). Concurring with the overall accuracy of 99.62% of this parameter, the class accuracies do not drop less than 93.66%, with Texture G (6 Sinusoidal waves) being the only one that caused some confusion for the SVM classifier. The soft biomimetic finger benefits from its pliancy and the spatial integration of the taxels in the flexible tactile sensor array when discriminating textures. These results confirm the robust and high performing texture discrimination capability of the neuromorphic encoding algorithm. Next, we demonstrate the resultant sensory feedback to the user.

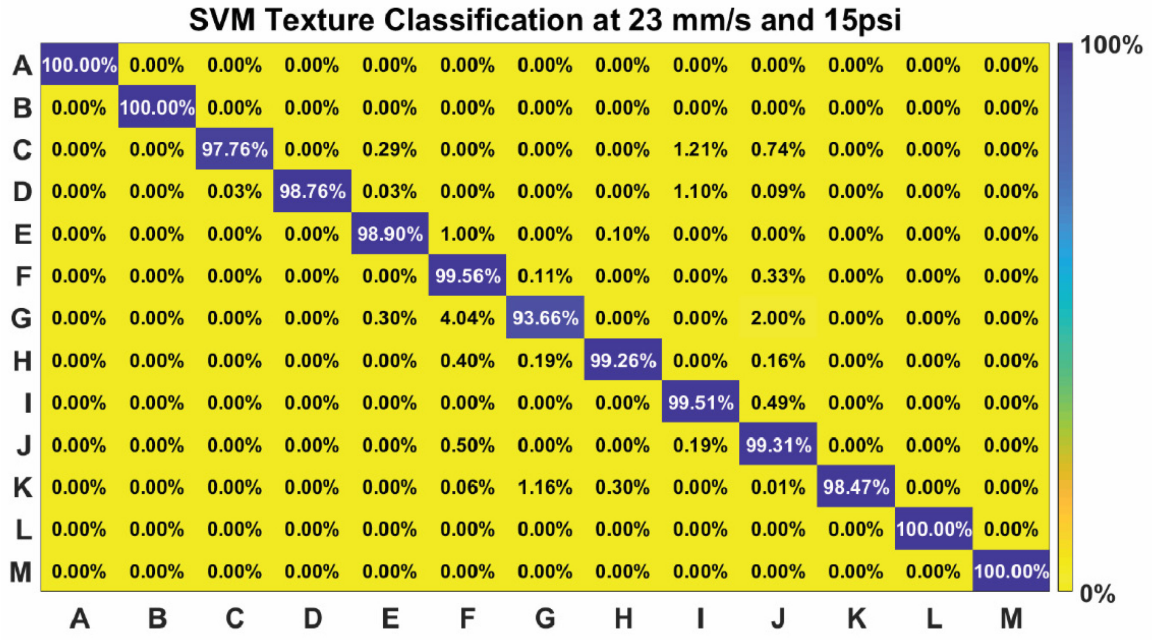

Figure 4.8: Confusion matrix showing the class accuracy of each texture when the soft biomimetic finger was actuated to 15 psi and palpated the textures at 23 mm/s. The soft biomimetic finger was able to successfully discriminate the textures at this parameter, achieving an overall classification accuracy of 99.62%.

4.3.3 Sensory Feedback

Three able-bodied subjects participated in the stimulation psychophysical experiments. The results of the conditional discrimination experiment are shown in Figure 4.9, where the rows represent the condition presented first and the columns represent the condition presented second. Subjects AB01 and AB02 were able to differentiate between three conditions, while subject AB03 was able to differentiate between two conditions. The ability to discriminate between stimulation frequencies or intensities varied among subjects. Subject AB01 had difficulty separating discrete versus continuous pattern at low stimulation intensity (Figure 4.9A). Subject AB02 had difficulty separating low versus high intensity for the continuous stimulation pattern (Figure 4.9B). Subject AB03,

however, could only determine the difference in discrete vs. continuous patterns, but not intensity (Figure 4.9C).

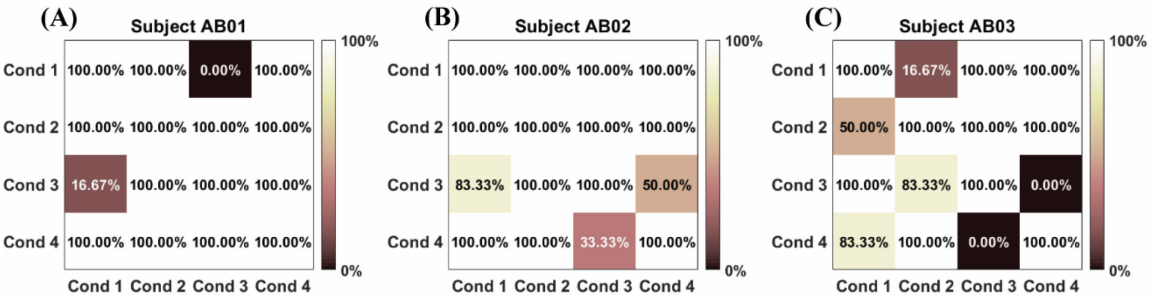

Figure 4.9: Condition discrimination results for subjects AB01 (A), AB02 (B), and AB03 (C). Each grid shows the percentage at which the subject was able to identify if the conditions presented were the same or different.

4.3.4 Comparison between Rigid and Soft Fingers

The texture discrimination experiment was also run using the same tactile sensor array attached to the fingertip of the index finger on a Touch Bionics prosthetic hand. This was done to compare how well the soft finger was able to classify soft and hard textures compared to a rigid finger. For this comparison, another set of textured plates, identical to those shown in Figure 4.4, were fabricated out of Dragon Skin™ 10 silicone, referred to as soft textured plates. The soft biomimetic finger and rigid prosthetic finger passively palpated these soft textured plates and the original hard textured plates, with 40 trials for each of the 26 textures.

Overall, the soft finger performed on par with the rigid finger, with a slight improvement at discriminating the soft textures. The soft finger achieved an accuracy of 98.65% for both soft and hard textures, while the rigid finger obtained an accuracy of 98.27% for hard textures and 97.31% for soft textures. Although the differences are small,

the drop in performance of soft texture discrimination for the hard finger could indicate the benefit of the soft finger to discriminate soft textures.

4.4 Discussion

A soft finger with a soft, compliant sensor and neuromorphic encoding attempts to mimic a human finger. Our study finds that this combination of features has many attributes of human fingers. The compliance of the soft finger would aid it in palpating softer materials. However, further exploration is needed to determine the relative benefits of our soft finger solution compared to the current hard finger design as the results from our limited study of textures between the two were comparable. Additionally, our study did not include objects of different curvature. Still, the benefits of the soft finger, such as suitability to handle delicate objects, could pave the way for a hybrid biomimetic or andromorphic finger solution, combining the advantages of both soft and hard materials.

Sensors incorporated into soft robots prioritize flexibility and simple fabrication to minimize its effect on the robot's actuation. Therefore, the primary design constraint of our sensor is that it needs to be flexible and cannot interfere with the normal actuation of the soft biomimetic finger. Based on this, we created a novel flexible, textile tactile sensor for the soft biomimetic finger, with neuromorphic output that performed well at texture discrimination.

With the current selection of textures, the soft finger was able to classify the textures with a high level of accuracy. A texture database, which includes finer natural textures, would help validate and test this method further [37]. Decoding algorithms such

as Victor Purpura distance and van Rossum distance with spiking neural networks can also provide more information about the textures and improve classification performance [30], [37]. Additionally, the design of the flexible tactile sensor array with overlapping receptor fields allows the use of super-resolution. By involving spatial averages over the taxels in the sensor array, the ability to sense at a higher acuity is possible. This is a technique used to enhance the resolution of an imaging system [137]. The human body is also able to perceive textures regardless of the speed of palpation. This speed invariance could be achieved using a modified neuromorphic model and testing with a similar method. Finally, by using multiple soft biomimetic fingers in unison, grasping and manipulating objects with texture recognition, while providing sensory feedback is possible.

Since the subjects were only able to differentiate between a few conditions, static stimulation using TENS may not be enough to convey all the current textural information. However, dynamic stimulation of the user with the neuromorphic output could convey more information. Using these sensory feedback methods, a more natural perception of the environment can occur and ultimately aid in prosthetic embodiment. Additionally, this work will be useful in human-machine interactions, such as co-robotics, especially as robotic hands and human hands interact.

Acknowledgment

This research was funded by a grant from the Office of Naval Research (Global) to the Singapore Institute of Neurotechnology and the NSF award 1830444 under the National Robotics Initiative to Johns Hopkins University.

Chapter 5

Continuing Work and Future Directions

This chapter summarizes the continuing work and future directions in which this work could potentially be taken forward.

5.1 Soft Tissue Palpation

Tactile sensing by palpation (Figure 5.1) is still used for diagnosing the early formation of malignant tumors and lumps to detect lymph nodes, and breast cancer [138]. However, tactile sensing-based diagnosis needs trained clinicians to perform palpation procedures and the interpretation of the results is highly subjective due to the lack of any quantitative measurement. Therefore, to assist physicians in detecting lumps more efficiently, various imaging techniques such as x-rays, ultrasonic imaging, and computer tomography have been developed [139], [140]. Though these imaging techniques offer an enhanced diagnosis of lumps or tumors, each of these techniques has limitations, including the exposure to radiation, excessive costs, and complexity of machinery [141]. In some studies, it is reported that imaging-based diagnosis such as mammography missed the

breast cancer that was later detected by clinical breast examination by palpation [142], [143]. Additionally, in some cases, the early formation of cancerous tissue has been perceived through palpation but failed to appear through medical imaging due to its small size or the high-density of the surrounding tissue surrounding. Therefore, palpation-based diagnosis has its relevance even in the age of digital imaging-based diagnosis of tumors and lymph nodes.

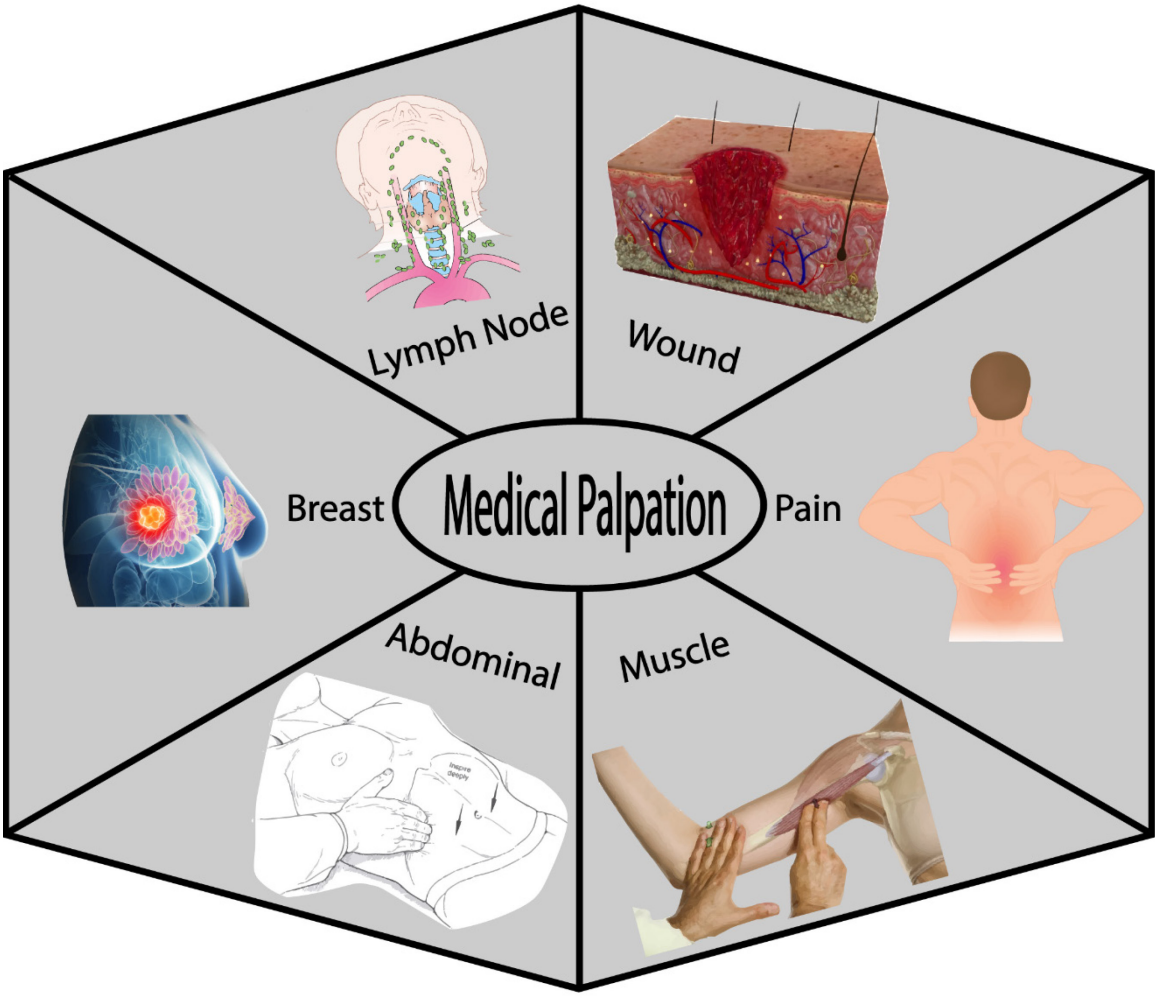

Figure 5.1: Different medical applications where palpation is used as a diagnostic tool.

Most of the existing tactile sensing devices for palpation have focused on either improving the sensitivity, the spatial density of tactile sensors, or developing sophisticated algorithms to process the tactile signals for diagnosis. However, these studies did not consider the mechanically and neurophysiologically complex process of tactile sensing through palpation using a human finger. The human tactile system uses sensory information gathered from four different types of mechanoreceptors embedded in the skin: Meissner corpuscles, Merkel cell, Pacinian corpuscles, and Ruffini endings.

5.1.1 Lymph node

This project aims to develop a bioinspired soft robotic palpation system for medical examination. Specifically, we want to address clinical palpation for lymph nodes in the human body. Lymph node palpation is an essential part of the evaluation for infectious diseases or cancer. Cervical lymph nodes are common sites for metastatic cancer in the neck and head cancer [144]. Although ultrasound assessment of cervical lymph nodes has been well established, palpation of cervical lymph nodes is still common in clinical practice [145]. However, palpation to gauge nodal hardness is considered inaccurate and carries substantial risks of misdiagnosis due to subjectivity in manual palpation [146]. Among other factors, the stiffness of the lymph node alone is enough for an accurate diagnosis of lymph node metastases [147]. Therefore, being able to quantitatively measure the relative or absolute stiffness of the lymph node can help the clinician make the right diagnosis. The goal of this research is to develop a bioinspired sensing and learning paradigm to estimate the mechanical properties of a nodule by palpation using a soft biomimetic finger with a sense of touch. The biomimetic tactile sensing can help us to quantitatively measure a

nodule's stiffness. In addition to tissue stiffness, geometric parameters such as size and depth of the stiff region are important factors for the proper diagnosis of the lymph node. The combined knowledge of lymph node stiffness and geometry would aid in identifying infectious or cancerous lymph nodes (lymphoma) and help physicians select an appropriate treatment strategy. We propose a biomimetic tactile sensing framework to detect and quantify various parameters such as stiffness, size, and depth of an embedded hard nodule with a geometric representative of lymph node pathology (Figure 5.2). To achieve this, we use finite element modeling (FEM) analysis to model the complex interaction between the soft finger augmented with a flexible tactile sensor and an idealized skin model with an embedded nodule of varying parameters. The FEM analysis will be used to generate simulated tactile responses corresponding to the different size, hardness, and depth of the embedded nodules in the skin model. These simulated tactile responses will then be used as input training data to an SNN-based learning paradigm to map the simulated tactile response to the nodule parameters. Subsequently, the developed SNN model will be validated by the realistic phantom tissue with inclusions to emulate the lymph nodes. Finally, experiments on animal models can be carried out to further validate this method.

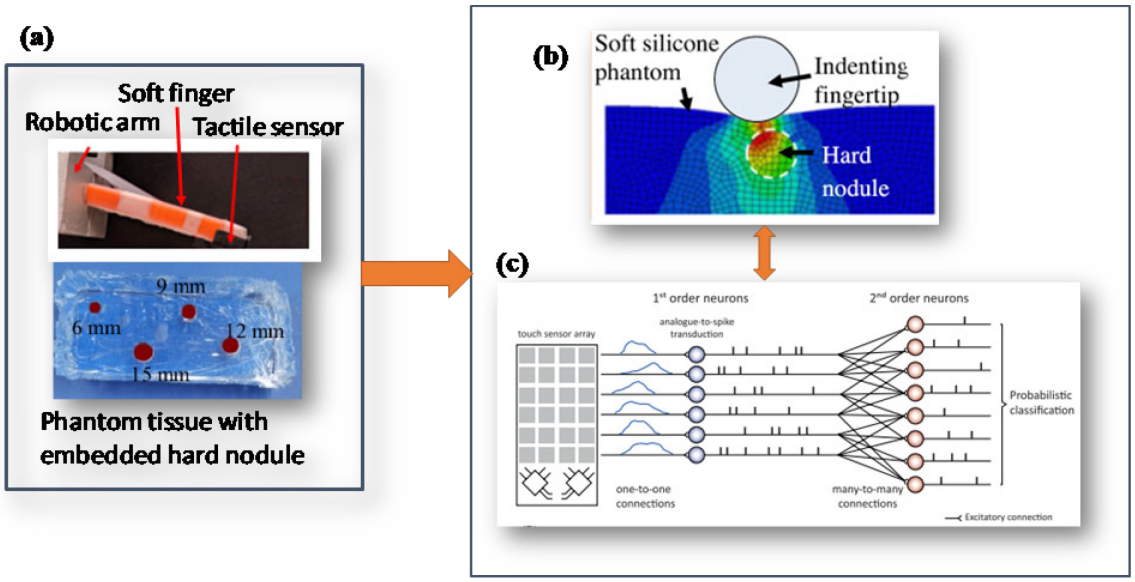

Figure 5.2: Proposed soft tissue palpation for lump detection using soft biomimetic finger and neuromorphic tactile sensing. **(a)** A soft finger with a fingertip tactile sensor attached to a robotic arm ready to palpate over the phantom tissue with the embedded hard nodule. **(b)** Modeling the complex mechanical interaction between soft finger and soft silicone phantom with the embedded hard nodule. **(c)** Spiking neural network architecture to mimic neurophysiological touch sensing and learning paradigm to classify different nodules.

For this project, the soft biomimetic finger using a flexible tactile sensor with some FEM analysis has been through some preliminary testing. The finished framework with complete experiments will be continued in the future.

5.1.2 Wound Palpation

Conventional wound care uses standard rulers and visual inspection to diagnose wounds and judge the healing process. Doctors and health specialists base treatment decisions on the initial status of the wound and subsequently, the progress of the wound. The main characteristics of the structure of the wound that needs to be imaged are visualizing the depth, volume, and the viability of the injured tissue and surround tissue. Wound imaging is useful as a diagnostic tool and to monitor and document the quality of

the wound. This is especially true for pressure ulcers and chronic wounds. MRI and CT are modalities that are too cost-prohibitive to analyze all regional wounds.

Recent technologies are having wound assessment capabilities with 3D wound measurement and composition. InSight by WoundWorks® and Tissue Analytics® record, track, and analyze patient wounds based on photography [148], [149]. These technologies can use machine learning to analyze and approximate wound tissue composition. However, standard 3D photography does not provide information about the underlying tissue, which could be injured in closed wounds with deep tissue injuries [150].

High-resolution ultrasound can provide visualization of the underlying tissue structure and vasculature for even deep tissue injuries. Current diagnostic ultrasound has promise but is not practical [150]. Recent advancements in ultrasound sensors arrays could create high sensitivity and resolution imaging of wounds to create a more practical wound assessment tool [151]–[155]. By adding other sensing modalities such as laser speckle contrast imaging and optical sensing, a more holistic characterization of the wound can occur. Laser speckle contrast imaging has been used in imaging for blood flow measurement for perfusion in tissues [156]. The standardization of measuring techniques in wound care using advanced imaging and sensing technologies can provide comprehensive information for wound diagnostics and management [150].

A proposed wound assessment tool can use multimodal sensing to diagnose, map, and predict the progression of wounds (Figure 5.3). An RGB camera, or thermal camera, will provide visual information about the wound such as its dimensions, tissue oxygenation, blood flow, and temperature. Tactile palpation will be used to inspect the

periwound through palpation to access the skin's integrity. Palpation can also provide information on the moisture, temperature, texture, turgor, pulses, and mobility of the wound and its surrounding tissue. By converting the output from the camera and tactile sensor into event-based spikes, the information from the two sources can be combined and used in an SSN. The SSN can use the tactile and vision data over time to predict wound recovery time.

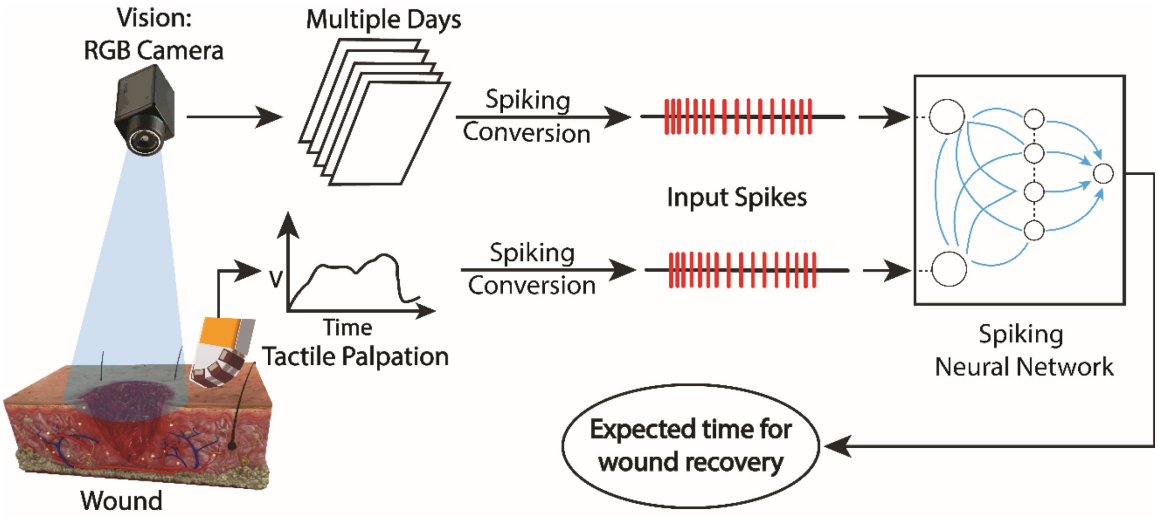

Figure 5.3: Proposed wound assessment tool using event-based visual and tactile sensing.

5.2 Embedded Multilayer Sensor

The goal of biomimetic tactile sensors is to mimic the mechanoreceptors in the skin. An alternative to merely increasing the spatial resolution of the sensor is creating a multilayer sensor, which can be used to ascertain essential information from an object or surface. By creating a multilayer tactile sensor, multiple neuromorphic encoding algorithms can be used to represent the varied mechanoreceptors. The current textile tactile sensor mimics only a single type of mechanoreceptor, Merkel cells. However, different

mechanoreceptors in the skin sense different distinct tactile information and are organized in different layers in the skin. A multilayer sensor allows for additional spatiotemporal information to be gathered from the object or surface.

A multilayer tactile sensor was designed using the 3x3 tactile sensor and an embedded 2x3 tactile sensor layer to mimic two types of mechanoreceptors found in human skin (Figure 5.4). The outer sensor layer has more taxels with smaller sensing areas (nine 4 mm^2 taxels) to mimic Merkel cells, while the embedded sensor layer is deeper and has fewer taxels with larger sensing areas (six 16mm^2 taxels) to mimic Pacinian corpuscles. Each of the receptors encodes different haptic features to create a biomimetic tactile sensor with the potential to provide amputees a sense of touch.

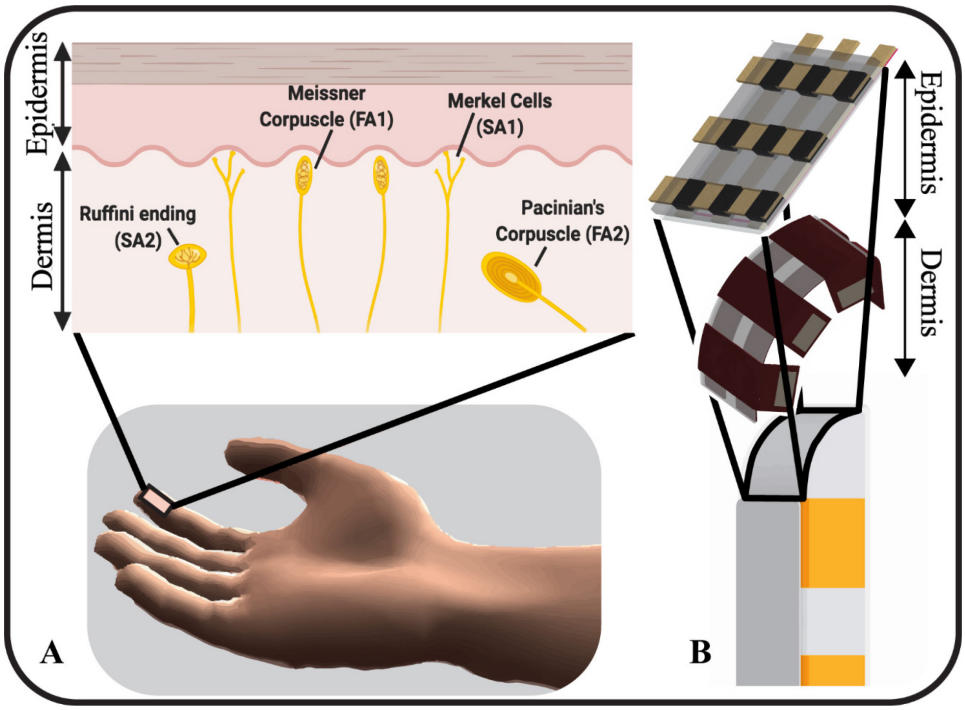

Figure 5.4: (A) Graphic depicting the mechanoreceptors in human skin. Merkel cells encode touch for coarse textures and Pacinian corpuscles encode vibration for finer textures. **(B)** multilayer tactile sensor attached to the soft biomimetic finger.

The multilayer sensor has been fabricated and ready to be integrated with the soft biomimetic finger. Complete calibration and texture discrimination experiments will be completed in the future and the results will be submitted to a conference.

5.3 Hybrid Soft Finger

Soft robots have many advantages over rigid robots due to their compliance. However, a completely soft finger with soft actuators cannot create the same level of force to grasp objects as its rigid counterpart. To create a biomimetic soft finger that can be incorporated into a prosthetic hand, a hybrid soft finger was designed. This hybrid soft biomimetic finger incorporates a rigid skeletal structure into the finger to improve its overall structural integrity and force output. The finger consists of three "Pneu-Nets" inspired pneumatic actuators with integrated air channels inside its strain-limiting bottom layer, as seen in Figure 5.5. These three actuators make up the actuation layer of the finger.

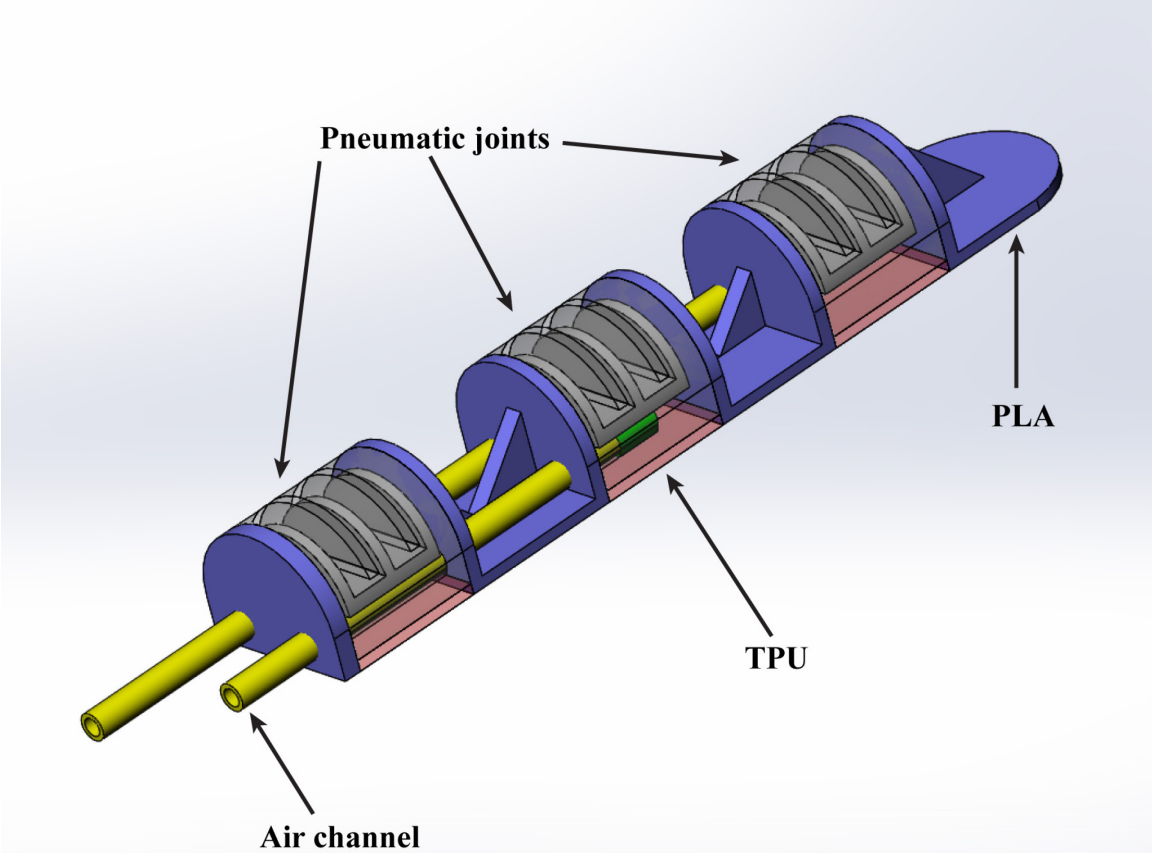

Figure 5.5: 3D model of the Hybrid soft biomimetic finger where the yellow represents the air tubes, green represents the 3D printed air channel adapters, red represents the TPU material, and Purple represents the PLA material.

The rigid "bone" layer consists of two different 3D printed materials, TPU in red and PLA in purple, as seen in Figure 5.6. TPU serves as a secondary strain limiting layer that allows the actuator to bend at the specified joint spots and the PLA parts are bonded to the actuators to transfer as much force as possible from the actuator inflation.

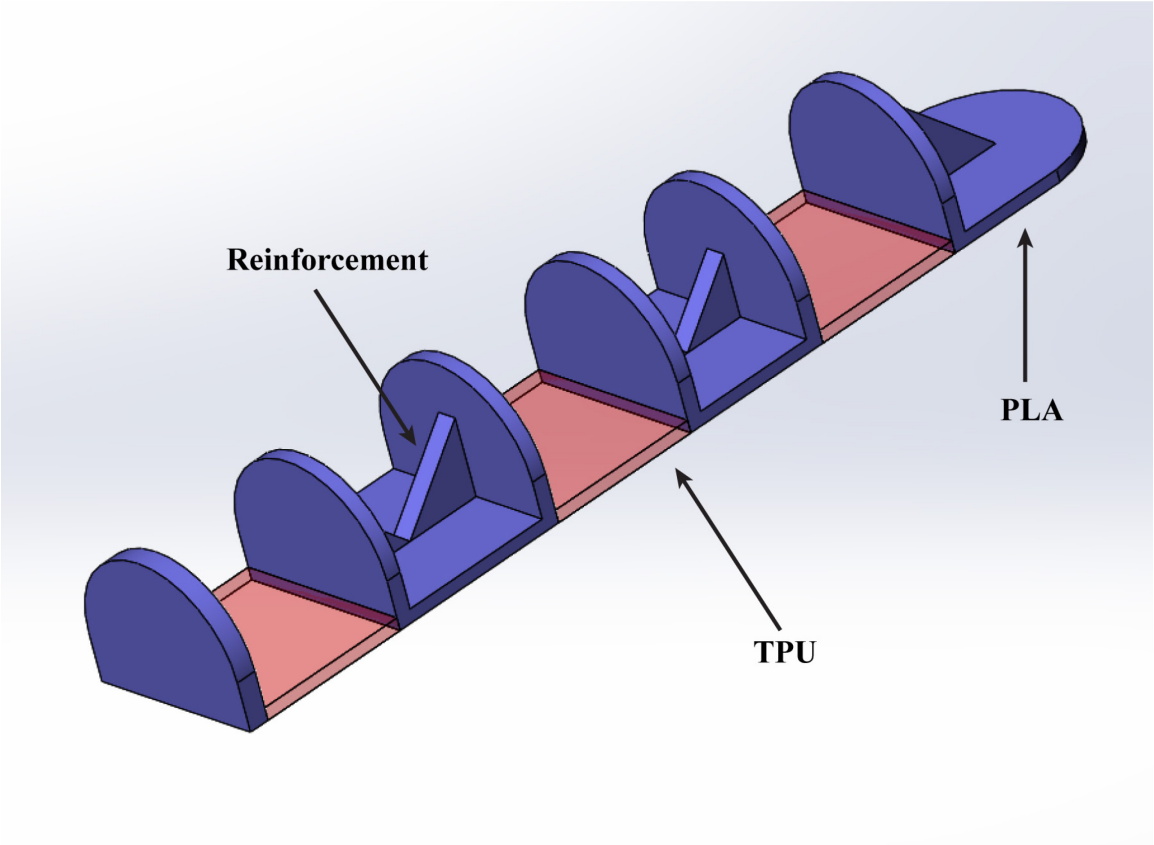

Figure 5.6: 3D model of the 'bone" layer of the hybrid soft biomimetic finger.

To compare the force output of the hybrid soft finger to the current soft finger, the fingers were modeled and analyzed through FEM simulations Figure 5.7. The following figures are preliminary simulation results of the hybrid soft finger in ANSYS Discovery AIM. The complete simulation analysis, with a comparison to the current soft finger, and fabrication of the hybrid soft finger are continuing and will be completed in the future.

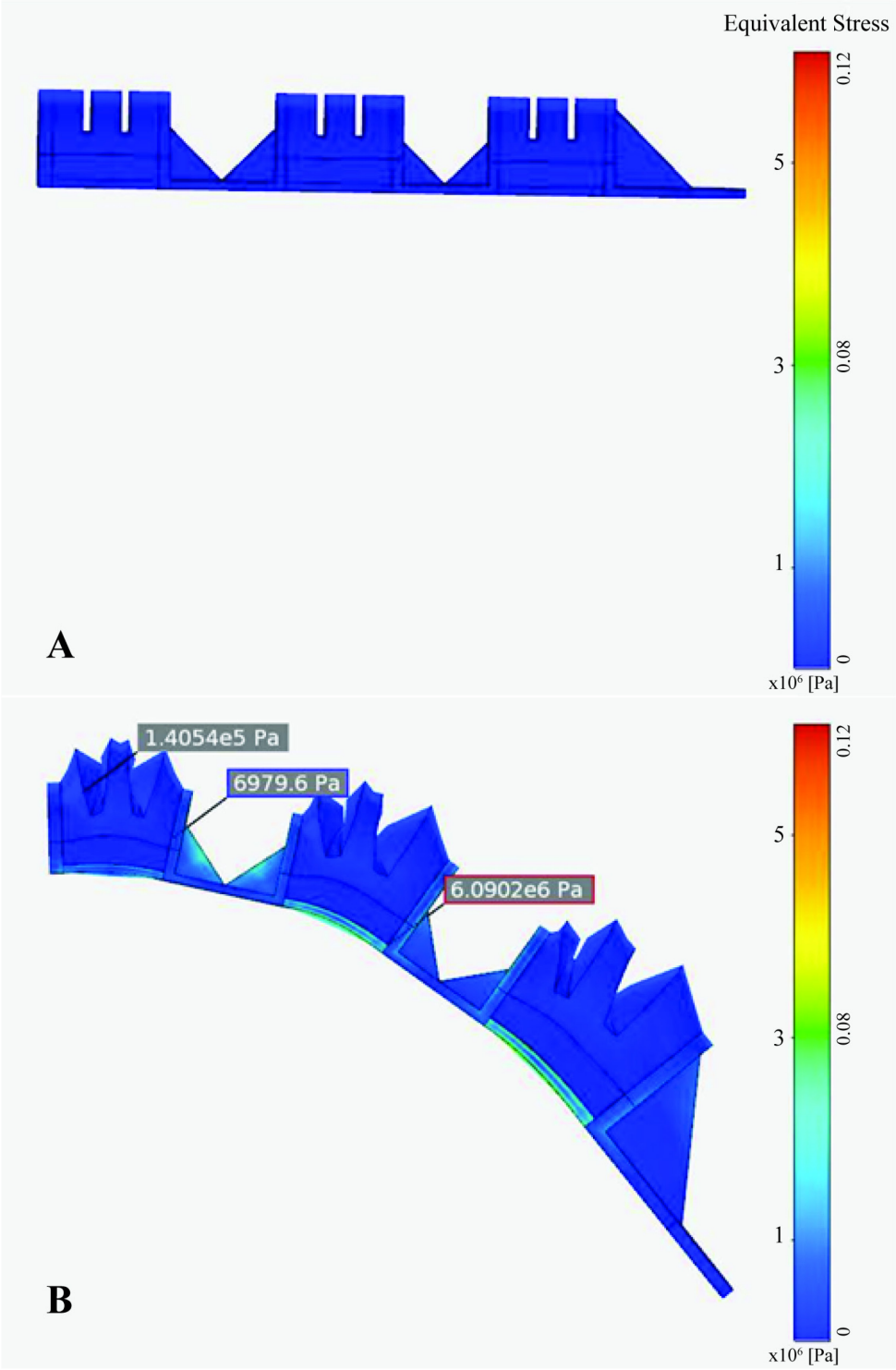

Figure 5.7: The Hybrid finger was simulated in ANSYS Discovery AIM. The finger was actuated at 15 psi in all three actuators and the stress was measured. Based on these results, no points of failure are noticeable in the model.

5.4 Pneumatic Actuation System

The current pneumatic setup (Fig. 5.8) for the soft biomimetic finger used an air compressor and two 3-way direct-acting solenoid valves to regulate the airflow into the soft biomimetic finger. Each valve is connected to an air channel's inlet and a pressure sensor (Honeywell ASDXACX100PAAA5). The pneumatic circuit is independently controlled by an Arduino microcontroller. However, this actuation method is an open system, where the compressor needs to be manually adjusted to achieve the desired pressure levels.

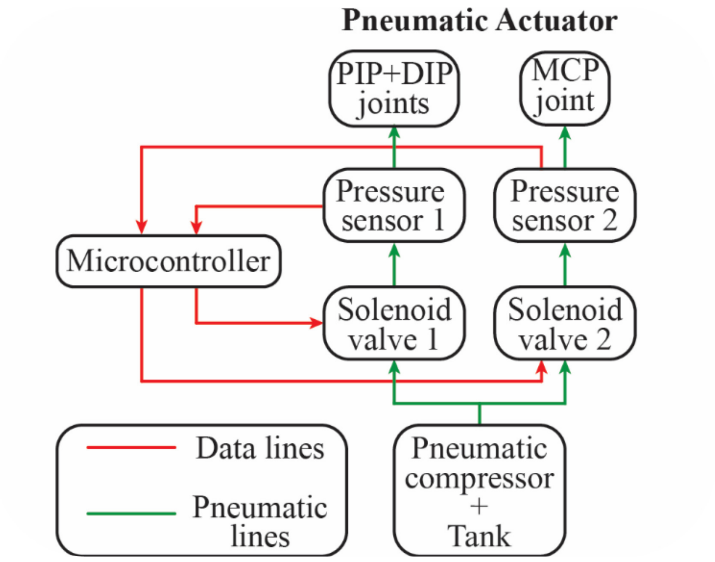

Figure 5.8: Overview of the pneumatic setup used to actuate the soft finger.

The goal of the soft biomimetic finger project is to ultimately create a soft prosthetic hand that an amputee can use. To achieve this goal, the actuation system of the soft biomimetic finger needs to be improved. The requirements for this are listed below:

1) Closed-loop actuation

2) Automatic release of air in fingers
3) Control at least 10 channels for 5 fingers
4) Portable actuation system
5) Control board that can incorporate sensing and sensory feedback

Currently, the actuation system is designed to control a single soft finger. (1) The closed-loop control involves creating a connection between the pressure sensor and a pressure regulator. This will allow the soft fingers to actuate to the desired pressure and thus bending angle. At its first stage, the soft fingers will need to achieve the desired bending angle set by the manual control, using rotary switches. The next stage involves controlling the actuation of the soft finger through software, such as Arduino. This will streamline the actuation of the soft prosthetic hand by creating the pathway for other control methods such as Electromyography (EMG). EMG is the most common method of controlling myoelectric prosthesis and will allow an upper-limb amputee to control the soft prosthetic hand. (2) Once the fingers have been actuated, the air needs to be manually released by the compressor. Using pressure regulators with a release will not only allow the system to precisely actuate to a desired pressure but also release the air in the soft finger to go back to rest. (3) To control 5 fingers that each has 2 independently actuated fingers, the actuation system needs to be scaled up. Ideally, this will use a single compressor and a pressure regulator for each of the 10 inlets. (4) The current pneumatic actuation system uses large components, such as compressors and solenoid valves. However, for a prosthetic hand, the actuation system needs to be miniaturized. While a fully miniaturized system that can fit in a socket may not be possible yet, a more portable system can be created. (5)

Instead of having multiple microcontrollers for actuation, sensing, and sensory stimulation, a singular microcontroller would be ideal. Additionally, compressors are bulky and not suitable for a portable system. Small compressed air canisters could be used instead to actuate the prosthetic hand. These could be comparable to swapping out batteries.

The following proposed design (Figure 5.9) was created by Josiah Kim, an intern in the lab. This is a theoretical design that has not been built or tested. The pneumatic actuation system project will be continued in the Fall of 2020 by another intern, Arnav Gupta.

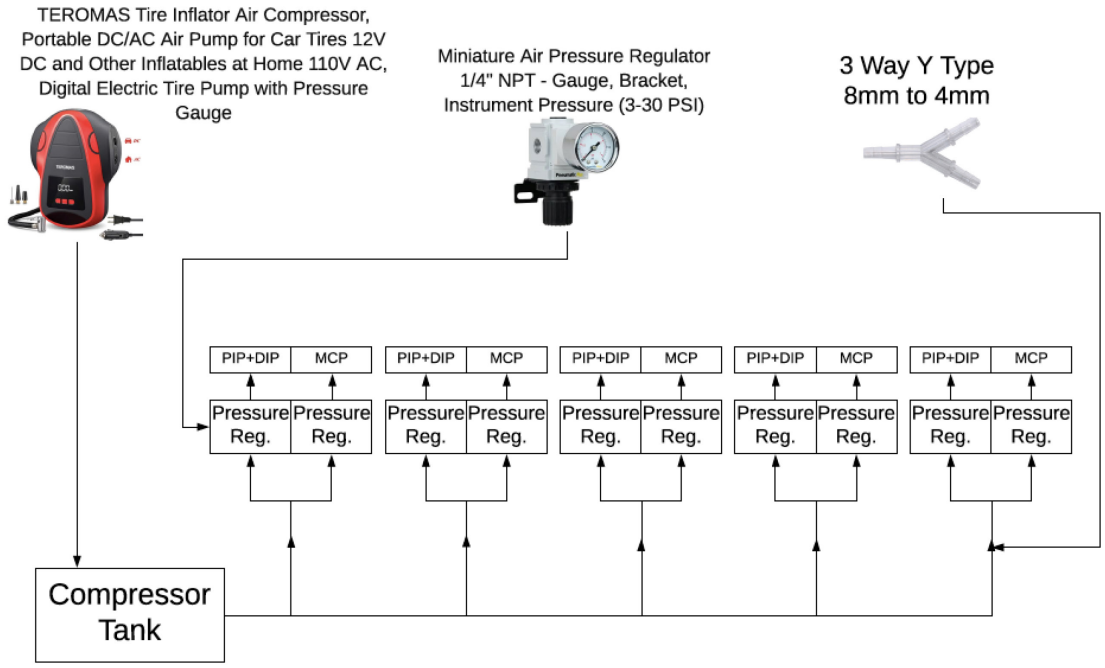

Figure 5.9: Proposed design of a pneumatic actuation system for a soft prosthetic hand.

5.5 Soft Prosthetic Hand

The overall goal is to create a soft prosthetic hand that an amputee can use in their daily lives and perceive their environment better. This biomimetic prosthetic hand will be compliant, with rigid structural support. Additionally, it would be controlled by EMG or ultrasound and will provide an amputee with a sense of touch. Each of the fingertips will have flexible multilayer sensors, with the potential for tactile sensing throughout the hand. The sensor output would be neuromorphically encoded and directly provide feedback to the amputee through TENS. Once the soft prosthetic hand is designed and constructed, it can be tested with amputee subjects doing functional assessments. A completed soft prosthetic hand would be a unique upper limb prosthesis with the potential to reduce the gap between a healthy arm and prosthesis by allowing users to improve their sense of touch while perceiving and interacting with their environment.

5.6 Multisensory Integration

The natural sensory feedback loop is an intuitive process for healthy individuals. Amputees with conventional prostheses lose the ability to feel when or how an object is being grasped and thus cannot adequately modulate their prosthetic hand movements based on natural sensory feedback [157], [158]. Replacement of this crucial loop starts with sensors that can detect various stimuli from the surrounding environment and the physical world. Tactile sensing of object stiffness and texture can be used to improve the breadth of sensations replaced for amputees while improving grasping tasks. Upon receiving static and dynamic sensory cues, the user can understand and dynamically interact with their surroundings [26], [27].

However, a single sensing modality is not sufficient to provide an amputee ample sensory information about their environment. To achieve human dexterity, the brain gathers information from multiple senses and integrates them to create a meaningful perceptual experience. This concept is known as multisensory integration and has been studied heavily in Neuroscience [159]–[162]. Concurrently, the approach of using multiple sensing modalities to improve object recognition and spatial mapping has been investigated for applications in robotics [163]–[171]. The valuable information obtained from multiple sensors can be merged to achieve a more accurate perception for amputees.

Though obtaining multimodal information through different sensors is not very complex, the challenge is trying to integrate all the varied information in a useful and efficient manner. The recent trend of deep learning, such as convolutional neural networks (CNN), and artificial intelligence (AI) have made this process more attainable [165], [172], [173]. Currently, the key issues with multimodal sensing are data synchronization and data fusion [174].

Tactile sensing can provide information about object texture and grasp, while vision can acquire information about object shape and location without contact. Therefore, the integration of visual and tactile information can be the most effective for coordinating a robotic arm or prosthesis for object manipulation [175]–[179]. Thus, the goal would be to use multisensory integration and AI to improve prosthesis for amputees.

5.7 High-density Sensor

The mechanoreceptors in human skin have a high spatiotemporal resolution to effectively manipulate objects. To achieve similar spatial information of mechanoreceptors, many tactile sensors and e-skins have been created with high resolutions [33], [44], [106], [180], [181]. However, the difficulty is being able to achieve such a high resolution and process the information and process it effectively. As the number of sensors increases, the serial transmission of data can become a bottleneck and limit the spatiotemporal information needed to effectively manipulate objects [180]. This time-divisional multiple access (TDMA) method is used by most tactile sensor arrays to transmit data, such as resistive row-column multiplexing [182]. Alternatively, event-based sensors using Address Event Representation (AER) or Asynchronously Coded Electronic Skin (ACES) only require signal transmission when necessary [180]. These protocols communicate with digital events containing the sensor value and address. By taking inspiration from the biological system and neuromorphically encoding multiple sensing elements, the information from a high-resolution sensor can be effectively used to provide an increased temporal resolution to discern transient events. Encoding temporal information is necessary because it provides crucial information when sensing fast-changing events. This biologically inspired neuromorphic encoding method can be used to multiplex numerous tactile sensors while retaining the necessary spatiotemporal information for rapid tactile sensing (Figure 5.10). This event-based data can be used with spiking neural networks (SNN) or extreme machine learning (ELM) to create reliable and robust tactile representation [33].

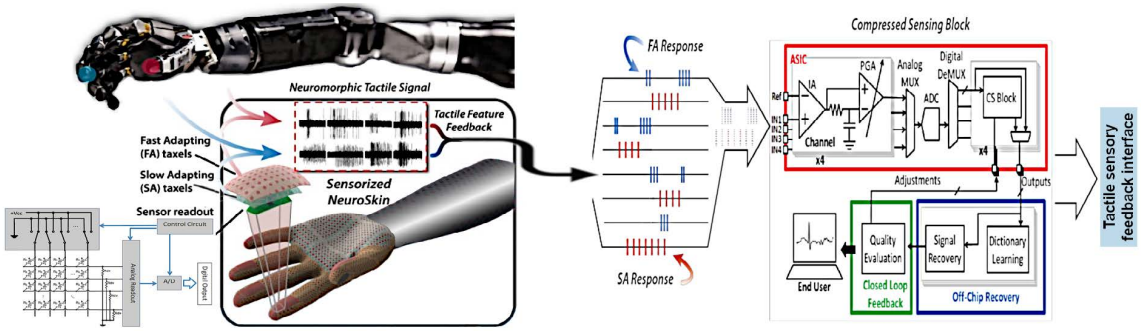

Figure 5.10: Neuromorphic approach for high-density touch sensing. From left to right: The fingertips and the palm of the prosthetic hand with the multilayer e-Dermis; An embedded flexible circuit (sensor readout) will acquire the data from the local sensor and convert it into neuromorphic spikes associated with the behavior of FA and SA taxels; A compressed sensing module will then encode tactile receptor inputs in space, depth profile, and timing.

5.8 Super Resolution

The design of the flexible tactile sensor array allows the ability to use super-resolution. By involving spatial averages over the taxels in the sensor array, the ability to sense at a higher acuity is possible (Figure 5.11). This is a technique used to enhance the resolution of an imaging system [137]. Such an approach can discern the necessary spatial information with a lower resolution sensor. Additionally, palpation can achieve a higher resolution through spatio-temporal receptor fields.

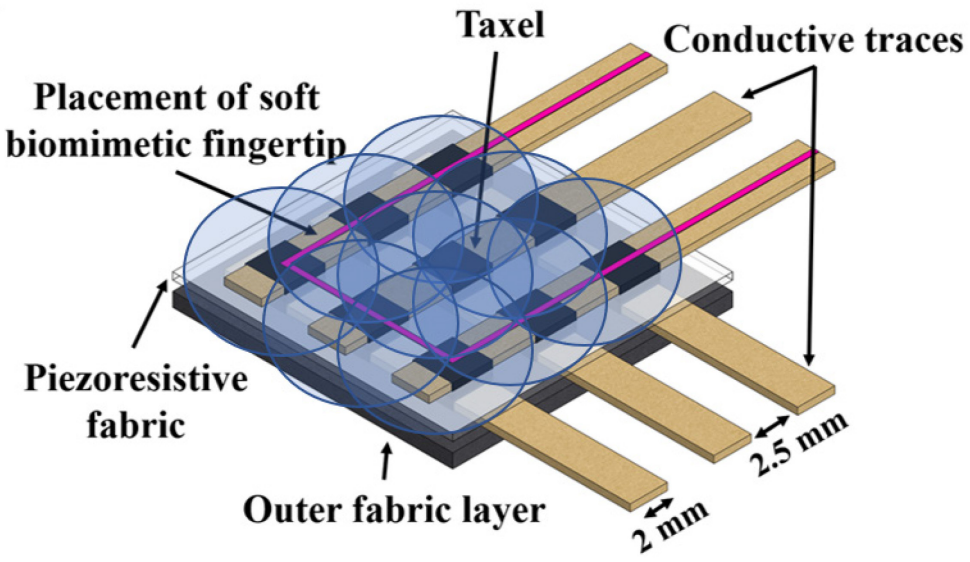

Figure 5.11: Overlapping receptor fields in the tactile sensor can allow spatial details in the subfield to be resolved by a population code.

5.9 Conclusion

Our word demonstrates the ability of the soft biomimetic finger to accurately differentiate textures with the added potential to provide users the ability to perceive their environment while interacting with it. The andromorphic nature of the soft biomimetic finger, with its softness, compliance, and neuromorphic mechanoreceptor-like spiking responses, make it best suited to bring robotic and prosthetic technology closer to a natural finger.

Furthermore, we showed that a novel soft, three-jointed biomimetic finger with 2 DOF and the ability to discriminate textures using a flexible textile tactile sensor array can palpate textures and then convey classified texture information to the user using sensory feedback. At different independent speeds of palpation and levels of actuation parameters, the soft biomimetic finger was able to classify textures with very high accuracy. Thus, our

work demonstrates the soft finger with biomimetic tactile sensors and neuromorphic encoding can be used for palpation applications, especially texture discrimination tasks.

Bibliography

[1] N. Sornkarn and T. Nanayakkara, "Can a Soft Robotic Probe Use Stiffness Control Like a Human Finger to Improve Efficacy of Haptic Perception?," *IEEE Trans. Haptics*, vol. 10, no. 2, pp. 183–195, Apr. 2017, doi: 10.1109/TOH.2016.2615924.

[2] H. Abidi *et al.*, "Highly dexterous 2-module soft robot for intra-organ navigation in minimally invasive surgery," *Int J Med Robotics Comput Assist Surg*, vol. 14, no. 1, p. e1875, Feb. 2018, doi: 10.1002/rcs.1875.

[3] A. Diodato *et al.*, "Soft Robotic Manipulator for Improving Dexterity in Minimally Invasive Surgery," *Surg Innov*, vol. 25, no. 1, pp. 69–76, Feb. 2018, doi: 10.1177/1553350617745953.

[4] A. Shiva *et al.*, "Tendon-Based Stiffening for a Pneumatically Actuated Soft Manipulator," *IEEE Robot. Autom. Lett.*, vol. 1, no. 2, pp. 632–637, Jul. 2016, doi: 10.1109/LRA.2016.2523120.

[5] P. Polygerinos, Z. Wang, K. C. Galloway, R. J. Wood, and C. J. Walsh, "Soft robotic glove for combined assistance and at-home rehabilitation," *Robotics and Autonomous Systems*, vol. 73, pp. 135–143, Nov. 2015, doi: 10.1016/j.robot.2014.08.014.

[6] Y.-L. Park *et al.*, "Design and control of a bio-inspired soft wearable robotic device for ankle–foot rehabilitation," *Bioinspir. Biomim.*, vol. 9, no. 1, p. 016007, Jan. 2014, doi: 10.1088/1748-3182/9/1/016007.

[7] J. J. Huaroto, E. Suarez, H. I. Krebs, P. D. Marasco, and E. A. Vela, "A Soft Pneumatic Actuator as a Haptic Wearable Device for Upper Limb Amputees: Toward a Soft Robotic Liner," *IEEE Robot. Autom. Lett.*, vol. 4, no. 1, pp. 17–24, Jan. 2019, doi: 10.1109/LRA.2018.2874379.

[8] E. Thompson-Bean, R. Das, and A. McDaid, "Methodology for designing and manufacturing complex biologically inspired soft robotic fluidic actuators: prosthetic hand case study," *Bioinspir. Biomim.*, vol. 11, no. 6, p. 066005, Oct. 2016, doi: 10.1088/1748-3190/11/6/066005.

[9] H. K. Yap *et al.*, "A Fully Fabric-Based Bidirectional Soft Robotic Glove for Assistance and Rehabilitation of Hand Impaired Patients," *IEEE Robot. Autom. Lett.*, vol. 2, no. 3, pp. 1383–1390, Jul. 2017, doi: 10.1109/LRA.2017.2669366.

[10] R. P. Rocha, P. A. Lopes, A. T. de Almeida, M. Tavakoli, and C. Majidi, "Fabrication and characterization of bending and pressure sensors for a soft prosthetic hand," *J. Micromech. Microeng.*, vol. 28, no. 3, p. 034001, Mar. 2018, doi: 10.1088/1361-6439/aaa1d8.

[11] Z. Shahid, A. L. Glatman, and S. C. Ryu, "Design of a Soft Composite Finger with Adjustable Joint Stiffness," *Soft Robotics*, p. soro.2018.0148, Aug. 2019, doi: 10.1089/soro.2018.0148.

[12] R. Deimel and O. Brock, “A novel type of compliant and underactuated robotic hand for dexterous grasping,” *The International Journal of Robotics Research*, vol. 35, no. 1–3, pp. 161–185, Jan. 2016, doi: 10.1177/0278364915592961.

[13] H. Zhao, K. O’Brien, S. Li, and R. F. Shepherd, “Optoelectronically innervated soft prosthetic hand via stretchable optical waveguides,” *Sci. Robot.*, vol. 1, no. 1, p. eaai7529, Dec. 2016, doi: 10.1126/scirobotics.aai7529.

[14] N. Feng, Q. Shi, H. Wang, J. Gong, C. Liu, and Z. Lu, “A soft robotic hand: design, analysis, sEMG control, and experiment,” *Int J Adv Manuf Technol*, vol. 97, no. 1–4, pp. 319–333, Jul. 2018, doi: 10.1007/s00170-018-1949-2.

[15] M. A. Devi, G. Udupa, and P. Sreedharan, “A novel underactuated multi-fingered soft robotic hand for prosthetic application,” *Robotics and Autonomous Systems*, vol. 100, pp. 267–277, Feb. 2018, doi: 10.1016/j.robot.2017.11.005.

[16] N. Feng, H. Wang, F. Hu, M. A. Gouda, J. Gong, and F. Wang, “A fiber-reinforced human-like soft robotic manipulator based on sEMG force estimation,” *Engineering Applications of Artificial Intelligence*, vol. 86, pp. 56–67, Nov. 2019, doi: 10.1016/j.engappai.2019.08.016.

[17] Z. Liang *et al.*, “High-Performance Flexible Tactile Sensor Enabling Intelligent Haptic Perception for a Soft Prosthetic Hand,” *Adv. Mater. Technol.*, vol. 4, no. 8, p. 1900317, Aug. 2019, doi: 10.1002/admt.201900317.

[18] J. Fras and K. Althoefer, “Soft Biomimetic Prosthetic Hand: Design, Manufacturing and Preliminary Examination,” in *2018 IEEE/RSJ International Conference on*

Intelligent Robots and Systems (IROS), Madrid, Oct. 2018, pp. 1–6, doi: 10.1109/IROS.2018.8593666.

[19] K. Suzumori, T. Maeda, H. Wantabe, and T. Hisada, "Fiberless flexible microactuator designed by finite-element method," *IEEE/ASME Trans. Mechatron.*, vol. 2, no. 4, pp. 281–286, Dec. 1997, doi: 10.1109/3516.653052.

[20] D. Trivedi, C. D. Rahn, W. M. Kier, and I. D. Walker, "Soft robotics: Biological inspiration, state of the art, and future research," *Applied Bionics and Biomechanics*, vol. 5, no. 3, pp. 99–117, Dec. 2008, doi: 10.1080/11762320802557865.

[21] C. Lee *et al.*, "Soft robot review," *Int. J. Control Autom. Syst.*, vol. 15, no. 1, pp. 3–15, Feb. 2017, doi: 10.1007/s12555-016-0462-3.

[22] R. L. Truby *et al.*, "Soft Somatosensitive Actuators via Embedded 3D Printing," *Adv. Mater.*, vol. 30, no. 15, p. 1706383, Apr. 2018, doi: 10.1002/adma.201706383.

[23] J. H. Low *et al.*, "Hybrid Tele-Manipulation System Using a Sensorized 3-D-Printed Soft Robotic Gripper and a Soft Fabric-Based Haptic Glove," *IEEE Robot. Autom. Lett.*, vol. 2, no. 2, pp. 880–887, Apr. 2017, doi: 10.1109/LRA.2017.2655559.

[24] O. S. Bholat, R. S. Haluck, R. H. Kutz, P. J. Gorman, and T. M. Krummel, "Defining the role of haptic feedback in minimally invasive surgery," *Stud Health Technol Inform*, vol. 62, pp. 62–66, 1999.

[25] R. Ong *et al.*, "A novel method for texture-mapping conoscopic surfaces for minimally invasive image-guided kidney surgery," *Int J CARS*, vol. 11, no. 8, pp. 1515–1526, Aug. 2016, doi: 10.1007/s11548-015-1339-2.

[26] R. S. Johansson and J. R. Flanagan, “Coding and use of tactile signals from the fingertips in object manipulation tasks,” *Nat Rev Neurosci*, vol. 10, no. 5, pp. 345–359, May 2009, doi: 10.1038/nrn2621.

[27] Z. Su, J. A. Fishel, T. Yamamoto, and G. E. Loeb, “Use of tactile feedback to control exploratory movements to characterize object compliance,” *Front. Neurorobot.*, vol. 6, 2012, doi: 10.3389/fnbot.2012.00007.

[28] D. Balamurugan *et al.*, “Texture Discrimination using a Soft Biomimetic Finger for Prosthetic Applications,” in *2019 IEEE 16th International Conference on Rehabilitation Robotics (ICORR)*, Toronto, ON, Canada, Jun. 2019, pp. 380–385, doi: 10.1109/ICORR.2019.8779442.

[29] S. Sankar *et al.*, “Texture Discrimination using a Flexible Tactile Sensor Array on a Soft Biomimetic Finger,” in *2019 IEEE SENSORS*, Montreal, QC, Canada, Oct. 2019, pp. 1–4, doi: 10.1109/SENSORS43011.2019.8956704.

[30] Z. Yi and Y. Zhang, “Recognizing Tactile Surface Roughness with a Biomimetic Fingertip: a Soft Neuromorphic Approach,” *Neurocomputing*, vol. 244, Mar. 2017, doi: 10.1016/j.neucom.2017.03.025.

[31] L. Qin and Y. Zhang, “Roughness Discrimination with Bio-inspired Tactile Sensor Manually Sliding on Polished Surfaces,” *Sensors and Actuators A: Physical*, vol. 279, Jun. 2018, doi: 10.1016/j.sna.2018.06.049.

[32] L. Qin, Z. Yi, and Y. Zhang, “Enhanced Surface Roughness Discrimination with Optimized Features from Bio-inspired Tactile Sensor,” *Sensors and Actuators A: Physical*, vol. 264, Jul. 2017, doi: 10.1016/j.sna.2017.07.054.

[33] M. Rasouli, Y. Chen, A. Basu, S. L. Kukreja, and N. V. Thakor, "An Extreme Learning Machine-Based Neuromorphic Tactile Sensing System for Texture Recognition," *IEEE Trans. Biomed. Circuits Syst.*, vol. 12, no. 2, pp. 313–325, Apr. 2018, doi: 10.1109/TBCAS.2018.2805721.

[34] S.-H. Kim, J. Engel, C. Liu, and D. L. Jones, "Texture classification using a polymer-based MEMS tactile sensor," *Journal of Micromechanics and Microengineering*, vol. 15, no. 5, pp. 912–920, May 2005, doi: 10.1088/0960-1317/15/5/003.

[35] S. Chun, Y. Kim, H.-S. Oh, G. Bae, and W. Park, "A highly sensitive pressure sensor using a double-layered graphene structure for tactile sensing," *Nanoscale*, vol. 7, no. 27, pp. 11652–11659, Jul. 2015, doi: 10.1039/C5NR00076A.

[36] S. Chun, A. Hong, Y. Choi, C. Ha, and W. Park, "A tactile sensor using a conductive graphene-sponge composite," *Nanoscale*, vol. 8, no. 17, pp. 9185–9192, Apr. 2016, doi: 10.1039/C6NR00774K.

[37] U. B. Rongala, A. Mazzoni, and C. M. Oddo, "Neuromorphic Artificial Touch for Categorization of Naturalistic Textures," *IEEE Trans. Neural Netw. Learning Syst.*, vol. 28, no. 4, pp. 819–829, Apr. 2017, doi: 10.1109/TNNLS.2015.2472477.

[38] Y. Cao, T. Li, Y. Gu, H. Luo, S. Wang, and T. Zhang, "Fingerprint-Inspired Flexible Tactile Sensor for Accurately Discerning Surface Texture," *Small*, vol. 14, no. 16, p. n/a, 2018, doi: 10.1002/smll.201703902.

[39] A. Song, Y. Han, H. Hu, and J. Li, "A Novel Texture Sensor for Fabric Texture Measurement and Classification," *IEEE Transactions on Instrumentation and*

Measurement, vol. 63, no. 7, pp. 1739–1747, Jul. 2014, doi: 10.1109/TIM.2013.2293812.

[40] N. Jamali and C. Sammut, "Majority Voting: Material Classification by Tactile Sensing Using Surface Texture," *IEEE Transactions on Robotics*, vol. 27, no. 3, pp. 508–521, Jun. 2011, doi: 10.1109/TRO.2011.2127110.

[41] H. B. Muhammad *et al.*, "A capacitive tactile sensor array for surface texture discrimination," *Microelectronic Engineering*, vol. 88, no. 8, pp. 1811–1813, 2011, doi: 10.1016/j.mee.2011.01.045.

[42] A. K. Gupta *et al.*, "A Neuromorphic Approach to Tactile Texture Recognition," in *2018 IEEE International Conference on Robotics and Biomimetics (ROBIO)*, Kuala Lumpur, Malaysia, Dec. 2018, pp. 1322–1328, doi: 10.1109/ROBIO.2018.8665085.

[43] A. Mazzoni, U. B. Rongala, and C. M. Oddo, "Decoding of naturalistic textures from spike patterns of neuromorphic artificial mechanoreceptors," *BMC Neurosci*, vol. 16, no. S1, pp. P186, 1471-2202-16-S1-P186, Dec. 2015, doi: 10.1186/1471-2202-16-S1-P186.

[44] L. E. Osborn *et al.*, "Prosthesis with neuromorphic multilayered e-dermis perceives touch and pain," *Sci. Robot.*, vol. 3, no. 19, p. eaat3818, Jun. 2018, doi: 10.1126/scirobotics.aat3818.

[45] S. Raspopovic *et al.*, "Restoring Natural Sensory Feedback in Real-Time Bidirectional Hand Prostheses," *Science Translational Medicine*, vol. 6, no. 222, pp. 222ra19-222ra19, Feb. 2014, doi: 10.1126/scitranslmed.3006820.

[46] H. Nguyen *et al.*, "Dynamic Texture Decoding Using a Neuromorphic Multilayer Tactile Sensor," in *2018 IEEE Biomedical Circuits and Systems Conference (BioCAS)*, Cleveland, OH, Oct. 2018, pp. 1–4, doi: 10.1109/BIOCAS.2018.8584826.

[47] M. M. Iskarous, H. H. Nguyen, L. E. Osborn, J. L. Betthauser, and N. V. Thakor, "Unsupervised Learning and Adaptive Classification of Neuromorphic Tactile Encoding of Textures," in *2018 IEEE Biomedical Circuits and Systems Conference (BioCAS)*, Cleveland, OH, Oct. 2018, pp. 1–4, doi: 10.1109/BIOCAS.2018.8584702.

[48] K. Suzumori, S. Endo, T. Kanda, N. Kato, and H. Suzuki, "A Bending Pneumatic Rubber Actuator Realizing Soft-bodied Manta Swimming Robot," in *Proceedings 2007 IEEE International Conference on Robotics and Automation*, Rome, Italy, Apr. 2007, pp. 4975–4980, doi: 10.1109/ROBOT.2007.364246.

[49] R. K. Katzschmann, A. D. Marchese, and D. Rus, "Hydraulic Autonomous Soft Robotic Fish for 3D Swimming," in *Experimental Robotics*, vol. 109, M. A. Hsieh, O. Khatib, and V. Kumar, Eds. Cham: Springer International Publishing, 2016, pp. 405–420.

[50] J. Walker *et al.*, "Soft Robotics: A Review of Recent Developments of Pneumatic Soft Actuators," *Actuators*, vol. 9, no. 1, p. 3, Jan. 2020, doi: 10.3390/act9010003.

[51] D. Balamurugan, "Soft Biomimetic Finger with Enhanced Sensing Capabilities for Prosthetic Application," *Johns Hopkins University*, vol. [Master's thesis], p. 162, May 2019.

[52] J. Amend, N. Cheng, S. Fakhouri, and B. Culley, “Soft Robotics Commercialization: Jamming Grippers from Research to Product,” *Soft Robotics*, vol. 3, no. 4, pp. 213–222, Dec. 2016, doi: 10.1089/soro.2016.0021.

[53] D.-Y. Lee, J.-S. Koh, J.-S. Kim, S.-W. Kim, and K.-J. Cho, “Deformable-wheel robot based on soft material,” *Int. J. Precis. Eng. Manuf.*, vol. 14, no. 8, pp. 1439–1445, Aug. 2013, doi: 10.1007/s12541-013-0194-8.

[54] A. Ainla, M. S. Verma, D. Yang, and G. M. Whitesides, “Soft, Rotating Pneumatic Actuator,” *Soft Robotics*, vol. 4, no. 3, pp. 297–304, Sep. 2017, doi: 10.1089/soro.2017.0017.

[55] T. Nagaoka, Z. Mao, K. Takemura, S. Yokota, and J. Kim, “ECF (electro-conjugate fluid) finger with bidirectional motion and its application to a flexible hand,” *Smart Mater. Struct.*, vol. 28, no. 2, p. 025032, Feb. 2019, doi: 10.1088/1361-665X/aaf49a.

[56] A. A. Stokes, R. F. Shepherd, S. A. Morin, F. Ilievski, and G. M. Whitesides, “A Hybrid Combining Hard and Soft Robots,” *Soft Robotics*, vol. 1, no. 1, pp. 70–74, Mar. 2014, doi: 10.1089/soro.2013.0002.

[57] Y. Shapiro, A. Wolf, and K. Gabor, “Bi-bellows: Pneumatic bending actuator,” *Sensors and Actuators A: Physical*, vol. 167, no. 2, pp. 484–494, Jun. 2011, doi: 10.1016/j.sna.2011.03.008.

[58] D. Yang *et al.*, “Buckling Pneumatic Linear Actuators Inspired by Muscle,” *Adv. Mater. Technol.*, vol. 1, no. 3, p. 1600055, Jun. 2016, doi: 10.1002/admt.201600055.

[59] Y. Elsayed *et al.*, "Finite Element Analysis and Design Optimization of a Pneumatically Actuating Silicone Module for Robotic Surgery Applications," *Soft Robotics*, vol. 1, no. 4, pp. 255–262, Dec. 2014, doi: 10.1089/soro.2014.0016.

[60] Y. Hwang, O. H. Paydar, and R. N. Candler, "Pneumatic microfinger with balloon fins for linear motion using 3D printed molds," *Sensors and Actuators A: Physical*, vol. 234, pp. 65–71, Oct. 2015, doi: 10.1016/j.sna.2015.08.008.

[61] S. Wakimoto, K. Suzumori, and K. Ogura, "Miniature Pneumatic Curling Rubber Actuator Generating Bidirectional Motion with One Air-Supply Tube," *Advanced Robotics*, vol. 25, no. 9–10, pp. 1311–1330, Jan. 2011, doi: 10.1163/016918611X574731.

[62] R. A. Bilodeau, E. L. White, and R. K. Kramer, "Monolithic fabrication of sensors and actuators in a soft robotic gripper," in *2015 IEEE/RSJ International Conference on Intelligent Robots and Systems (IROS)*, Hamburg, Germany, Sep. 2015, pp. 2324–2329, doi: 10.1109/IROS.2015.7353690.

[63] S. Sankar *et al.*, "Texture Discrimination using a Flexible Tactile Sensor Array on a Soft Biomimetic Finger," in *2019 IEEE SENSORS*, Montreal, QC, Canada, Oct. 2019, pp. 1–4, doi: 10.1109/SENSORS43011.2019.8956704.

[64] M. Schaffner, J. A. Faber, L. Pianegonda, P. A. Rühs, F. Coulter, and A. R. Studart, "3D printing of robotic soft actuators with programmable bioinspired architectures," *Nat Commun*, vol. 9, no. 1, p. 878, Dec. 2018, doi: 10.1038/s41467-018-03216-w.

[65] H. K. Yap, H. Y. Ng, and C.-H. Yeow, "High-Force Soft Printable Pneumatics for Soft Robotic Applications," *Soft Robotics*, vol. 3, no. 3, pp. 144–158, Sep. 2016, doi: 10.1089/soro.2016.0030.

[66] B. N. Peele, T. J. Wallin, H. Zhao, and R. F. Shepherd, "3D printing antagonistic systems of artificial muscle using projection stereolithography," *Bioinspir. Biomim.*, vol. 10, no. 5, p. 055003, Sep. 2015, doi: 10.1088/1748-3190/10/5/055003.

[67] D. B. Comber, J. E. Slightam, E. J. Barth, V. R. Gervasi, and R. J. Webster, "Design and Precision Control of an MR-Compatible Flexible Fluidic Actuator," in *ASME/BATH 2013 Symposium on Fluid Power and Motion Control*, Sarasota, Florida, USA, Oct. 2013, p. V001T01A048, doi: 10.1115/FPMC2013-4481.

[68] R. Niiyama, X. Sun, C. Sung, B. An, D. Rus, and S. Kim, "Pouch Motors: Printable Soft Actuators Integrated with Computational Design," *Soft Robotics*, vol. 2, no. 2, pp. 59–70, Jun. 2015, doi: 10.1089/soro.2014.0023.

[69] D. K. Patel, A. H. Sakhaei, M. Layani, B. Zhang, Q. Ge, and S. Magdassi, "Highly Stretchable and UV Curable Elastomers for Digital Light Processing Based 3D Printing," *Adv. Mater.*, vol. 29, no. 15, p. 1606000, Apr. 2017, doi: 10.1002/adma.201606000.

[70] H. Zhao, Y. Li, A. Elsamadisi, and R. Shepherd, "Scalable manufacturing of high force wearable soft actuators," *Extreme Mechanics Letters*, vol. 3, pp. 89–104, Jun. 2015, doi: 10.1016/j.eml.2015.02.006.

[71] H. Banerjee and H. Ren, “Optimizing Double-Network Hydrogel for Biomedical Soft Robots,” *Soft Robotics*, vol. 4, no. 3, pp. 191–201, Sep. 2017, doi: 10.1089/soro.2016.0059.

[72] H. Yuk, S. Lin, C. Ma, M. Takaffoli, N. X. Fang, and X. Zhao, “Hydraulic hydrogel actuators and robots optically and sonically camouflaged in water,” *Nat Commun*, vol. 8, no. 1, p. 14230, Apr. 2017, doi: 10.1038/ncomms14230.

[73] A. H. Velders, J. A. Dijksman, and V. Saggiomo, “Hydrogel Actuators as Responsive Instruments for Cheap Open Technology (HARICOT),” *Applied Materials Today*, vol. 9, pp. 271–275, Dec. 2017, doi: 10.1016/j.apmt.2017.08.001.

[74] K. K. Westbrook and H. J. Qi, “Actuator Designs using Environmentally Responsive Hydrogels,” *Journal of Intelligent Material Systems and Structures*, vol. 19, no. 5, pp. 597–607, May 2008, doi: 10.1177/1045389X07077856.

[75] N. Bassik, B. T. Abebe, K. E. Laflin, and D. H. Gracias, “Photolithographically patterned smart hydrogel based bilayer actuators,” *Polymer*, vol. 51, no. 26, pp. 6093–6098, Dec. 2010, doi: 10.1016/j.polymer.2010.10.035.

[76] I. D. Walker *et al.*, “Continuum robot arms inspired by cephalopods,” Orlando, Florida, USA, May 2005, p. 303, doi: 10.1117/12.606201.

[77] “Electroactive polymers.” https://promo.parker.com/parkerimages/promosite/ArtificialMuscle/UNITED%20STATES/About%20Electroactive%20Polymer/PDF/EAP Bulletin. pdf.

[78] “Electroactive polymers.” https://en.wikipedia.org/wiki/Electroactive polymers.

[79] R. Niiyama, D. Rus, and S. Kim, “Pouch Motors: Printable/inflatable soft actuators for robotics,” in *2014 IEEE International Conference on Robotics and Automation (ICRA)*, Hong Kong, China, May 2014, pp. 6332–6337, doi: 10.1109/ICRA.2014.6907793.

[80] J. Paek, I. Cho, and J. Kim, “Microrobotic tentacles with spiral bending capability based on shape-engineered elastomeric microtubes,” *Sci Rep*, vol. 5, no. 1, p. 10768, Sep. 2015, doi: 10.1038/srep10768.

[81] E. A. Allen, L. D. Taylor, and J. P. Swensen, “Smart Material Composites for Discrete Stiffness Materials,” in *Volume 2: Mechanics and Behavior of Active Materials; Structural Health Monitoring; Bioinspired Smart Materials and Systems; Energy Harvesting; Emerging Technologies*, San Antonio, Texas, USA, Sep. 2018, p. V002T06A015, doi: 10.1115/SMASIS2018-8203.

[82] N. Napp, B. Araki, M. T. Tolley, R. Nagpal, and R. J. Wood, “Simple passive valves for addressable pneumatic actuation,” in *2014 IEEE International Conference on Robotics and Automation (ICRA)*, Hong Kong, China, May 2014, pp. 1440–1445, doi: 10.1109/ICRA.2014.6907041.

[83] K. Elgeneidy, N. Lohse, and M. Jackson, “Bending angle prediction and control of soft pneumatic actuators with embedded flex sensors – A data-driven approach,” *Mechatronics*, vol. 50, pp. 234–247, Apr. 2018, doi: 10.1016/j.mechatronics.2017.10.005.

[84] R. F. Shepherd *et al.*, "Multigait soft robot," *Proceedings of the National Academy of Sciences*, vol. 108, no. 51, pp. 20400–20403, Dec. 2011, doi: 10.1073/pnas.1116564108.

[85] D. B. Camarillo, C. R. Carlson, and J. K. Salisbury, "Configuration Tracking for Continuum Manipulators With Coupled Tendon Drive," *IEEE Trans. Robot.*, vol. 25, no. 4, pp. 798–808, Aug. 2009, doi: 10.1109/TRO.2009.2022426.

[86] H.-T. Lin, G. G. Leisk, and B. A. Trimmer, "Soft Robots in Space: A Perspective for Soft Robotics," *ACT-PUB-AF06*, no. 06, pp. 69–79, 2013, doi: 10.2420/AF06.2013.69.

[87] C. D. Onal and D. Rus, "Autonomous undulatory serpentine locomotion utilizing body dynamics of a fluidic soft robot," *Bioinspir. Biomim.*, vol. 8, no. 2, p. 026003, Mar. 2013, doi: 10.1088/1748-3182/8/2/026003.

[88] E. Coevoet *et al.*, "Software toolkit for modeling, simulation, and control of soft robots," *Advanced Robotics*, vol. 31, no. 22, pp. 1208–1224, Nov. 2017, doi: 10.1080/01691864.2017.1395362.

[89] S. Mousavi, D. Howard, S. Wu, and C. Wang, "An Ultrasensitive 3D Printed Tactile Sensor for Soft Robotics," *arXiv:1810.09236 [physics]*, Sep. 2018, [Online]. Available: http://arxiv.org/abs/1810.09236.

[90] H. Devaraj, K. Yellapantula, M. Stratta, A. McDaid, and K. Aw, "Embedded piezoresistive pressure sensitive pillars from piezoresistive carbon black composites towards a soft large-strain compressive load sensor," *Sensors and Actuators A: Physical*, vol. 285, pp. 645–651, Jan. 2019, doi: 10.1016/j.sna.2018.12.006.

[91] E. L. White, J. C. Case, and R. K. Kramer, “Multi-mode strain and curvature sensors for soft robotic applications,” *Sensors and Actuators A: Physical*, vol. 253, pp. 188–197, Jan. 2017, doi: 10.1016/j.sna.2016.11.031.

[92] Y. Zhou, B. He, Z. Yan, Y. Shang, Q. Wang, and Z. Wang, “Touch Locating and Stretch Sensing Studies of Conductive Hydrogels with Applications to Soft Robots,” *Sensors*, vol. 18, no. 2, p. 569, Feb. 2018, doi: 10.3390/s18020569.

[93] B. Shih *et al.*, “Custom soft robotic gripper sensor skins for haptic object visualization,” in *2017 IEEE/RSJ International Conference on Intelligent Robots and Systems (IROS)*, Vancouver, BC, Sep. 2017, pp. 494–501, doi: 10.1109/IROS.2017.8202199.

[94] B. Shih *et al.*, “Design Considerations for 3D Printed, Soft, Multimaterial Resistive Sensors for Soft Robotics,” *Front. Robot. AI*, vol. 6, p. 30, Apr. 2019, doi: 10.3389/frobt.2019.00030.

[95] S. Ozel, N. A. Keskin, D. Khea, and C. D. Onal, “A precise embedded curvature sensor module for soft-bodied robots,” *Sensors and Actuators A: Physical*, vol. 236, pp. 349–356, Dec. 2015, doi: 10.1016/j.sna.2015.09.041.

[96] T. Paulino *et al.*, “Low-cost 3-axis soft tactile sensors for the human-friendly robot Vizzy,” in *2017 IEEE International Conference on Robotics and Automation (ICRA)*, Singapore, Singapore, May 2017, pp. 966–971, doi: 10.1109/ICRA.2017.7989118.

[97] H. Wang *et al.*, “Design Methodology for Magnetic Field-Based Soft Tri-Axis Tactile Sensors,” *Sensors*, vol. 16, no. 9, p. 1356, Aug. 2016, doi: 10.3390/s16091356.

[98] Y. He, X. Zhang, L. Zhu, G. Sun, X. Lou, and M. Dong, "Optical Fiber Sensor Performance Evaluation in Soft Polyimide Film with Different Thickness Ratios," *Sensors*, vol. 19, no. 4, p. 790, Feb. 2019, doi: 10.3390/s19040790.

[99] Q. Wang, X. Zhou, H. Jiang, G. Sun, and L. Zhu, "Polyimide sensing layer for bending shape measurement in soft surgical manipulators," *Optik*, vol. 183, pp. 179–188, Apr. 2019, doi: 10.1016/j.ijleo.2019.02.095.

[100] S. Sareh, Y. Noh, M. Li, T. Ranzani, H. Liu, and K. Althoefer, "Macrobend optical sensing for pose measurement in soft robot arms," *Smart Mater. Struct.*, vol. 24, no. 12, p. 125024, Dec. 2015, doi: 10.1088/0964-1726/24/12/125024.

[101] A. Masteller, S. Sankar, H. B. Kim, K. Ding, X. Liu, and A. H. All, "Recent Developments in Prosthesis Sensors, Texture Recognition, and Sensory Stimulation for Upper Limb Prostheses," *Annals of Biomedical Engineering*, vol. In review, Feb. 2020.

[102] B. C.-K. Tee *et al.*, "A skin-inspired organic digital mechanoreceptor," *Science*, vol. 350, no. 6258, pp. 313–316, Oct. 2015, doi: 10.1126/science.aaa9306.

[103] J. C. Yeo, Z. Liu, Z. Zhang, P. Zhang, Z. Wang, and C. T. Lim, "Wearable Mechanotransduced Tactile Sensor for Haptic Perception," *Advanced Materials Technologies*, vol. 2, no. 6, p. n/a, 2017, doi: 10.1002/admt.201700006.

[104] Z. Yi and Y. Zhang, "Bio-inspired Tactile FA-I Spiking Generation under Sinusoidal Stimuli," *Journal of Bionic Engineering*, vol. 13, no. 4, pp. 612–621, Oct. 2016, doi: 10.1016/S1672-6529(16)60332-3.

[105] K.-Y. Chun, Y. J. Son, E.-S. Jeon, S. Lee, and C.-S. Han, "A Self-Powered Sensor Mimicking Slow- and Fast-Adapting Cutaneous Mechanoreceptors," *Advanced Materials*, vol. 30, no. 12, p. 1706299, Mar. 2018, doi: 10.1002/adma.201706299.

[106] J. Kim *et al.*, "Stretchable silicon nanoribbon electronics for skin prosthesis," *Nature Communications*, vol. 5, no. 1, Dec. 2014, doi: 10.1038/ncomms6747.

[107] Z. Zou, C. Zhu, Y. Li, X. Lei, W. Zhang, and J. Xiao, "Rehealable, fully recyclable, and malleable electronic skin enabled by dynamic covalent thermoset nanocomposite," *Science Advances*, vol. 4, no. 2, p. eaaq0508, Feb. 2018, doi: 10.1126/sciadv.aaq0508.

[108] V. E. Abraira and D. D. Ginty, "The Sensory Neurons of Touch," *Neuron*, vol. 79, no. 4, pp. 618–639, Aug. 2013, doi: 10.1016/j.neuron.2013.07.051.

[109] S.-H. Kim, J. Engel, C. Liu, and D. L. Jones, "Texture classification using a polymer-based MEMS tactile sensor," *Journal of Micromechanics and Microengineering*, vol. 15, no. 5, pp. 912–920, May 2005, doi: 10.1088/0960-1317/15/5/003.

[110] Z. Liao *et al.*, "A tactile sensor translating texture and sliding motion information into electrical pulses," *Nanoscale*, vol. 7, no. 24, pp. 10801–10806, 2015, doi: 10.1039/C5NR01509J.

[111] L. Osborn, H. Nguyen, J. Betthauser, R. Kaliki, and N. Thakor, "Biologically inspired multi-layered synthetic skin for tactile feedback in prosthetic limbs," in *2016 38th Annual International Conference of the IEEE Engineering in Medicine and*

Biology Society (EMBC), Orlando, FL, USA, Aug. 2016, pp. 4622–4625, doi: 10.1109/EMBC.2016.7591757.

[112] A. Cranny, D. P. J. Cotton, P. H. Chappell, S. P. Beeby, and N. M. White, "Thick-film force and slip sensors for a prosthetic hand," *Sensors and Actuators A: Physical*, vol. 123–124, pp. 162–171, Sep. 2005, doi: 10.1016/j.sna.2005.02.015.

[113] D. He, W. Liu, Y. Ruan, X. Fu, and C. Stefanini, "Preliminary study on piezoresistive and piezoelectric properties of a double-layer soft material for tactile sensing," *ms*, vol. 21, no. 2, pp. 238–243, Jun. 2015, doi: 10.5755/j01.ms.21.2.6454.

[114] R. Kilaru, Z. Celik-Butler, D. P. Butler, and I. E. Gonenli, "NiCr MEMS Tactile Sensors Embedded in Polyimide Toward Smart Skin," *J. Microelectromech. Syst.*, vol. 22, no. 2, pp. 349–355, Apr. 2013, doi: 10.1109/JMEMS.2012.2222867.

[115] N. Lu, C. Lu, S. Yang, and J. Rogers, "Highly Sensitive Skin-Mountable Strain Gauges Based Entirely on Elastomers," *Adv.Funct.Mater.*, vol. 22, no. 19, pp. 4044–4050, 2012, doi: 10.1002/adfm.201200498.

[116] Z. Ji *et al.*, "The Design and Characterization of a Flexible Tactile Sensing Array for Robot Skin," *Sensors (Basel, Switzerland)*, vol. 16, no. 12, p. 2001, 2016, doi: 10.3390/s16122001.

[117] Y. Wu *et al.*, "A skin-inspired tactile sensor for smart prosthetics," *Science Robotics*, p. 9, 2018, doi: 10.1126/scirobotics.aat0429.

[118] H. Zhao, K. O'Brien, S. Li, and R. F. Shepherd, "Optoelectronically innervated soft prosthetic hand via stretchable optical waveguides," *Science Robotics*, vol. 1, no. 1, p. eaai7529, Dec. 2016, doi: 10.1126/scirobotics.aai7529.

[119] P. Yu, W. Liu, C. Gu, X. Cheng, and X. Fu, “Flexible Piezoelectric Tactile Sensor Array for Dynamic Three-Axis Force Measurement,” *Sensors*, vol. 16, no. 6, p. 819, Jun. 2016, doi: 10.3390/s16060819.

[120] H. B. Muhammad *et al.*, “Development of a bioinspired MEMS based capacitive tactile sensor for a robotic finger,” *Sensors & Actuators: A. Physical*, vol. 165, no. 2, pp. 221–229, 2011, doi: 10.1016/j.sna.2010.10.025.

[121] L. Zou, C. Ge, Z. J. Wang, E. Cretu, and X. Li, “Novel Tactile Sensor Technology and Smart Tactile Sensing Systems: A Review,” *Sensors (Basel, Switzerland)*, vol. 17, no. 11, p. 2653, 2017, doi: 10.3390/s17112653.

[122] C. Lucarotti, C. M. Oddo, N. Vitiello, and M. C. Carrozza, “Synthetic and bio-artificial tactile sensing: a review,” *Sensors (Basel, Switzerland)*, vol. 13, no. 2, pp. 1435–1466, 2013, doi: 10.3390/s130201435.

[123] P. Laszczak, L. Jiang, D. L. Bader, D. Moser, and S. Zahedi, “Development and validation of a 3D-printed interfacial stress sensor for prosthetic applications,” *Medical Engineering & Physics*, vol. 37, no. 1, pp. 132–137, Jan. 2015, doi: 10.1016/j.medengphy.2014.10.002.

[124] G. Liang, Y. Wang, D. Mei, K. Xi, and Z. Chen, “Flexible Capacitive Tactile Sensor Array With Truncated Pyramids as Dielectric Layer for Three-Axis Force Measurement,” *J. Microelectromech. Syst.*, vol. 24, no. 5, pp. 1510–1519, Oct. 2015, doi: 10.1109/JMEMS.2015.2418095.

[125] D.-H. Kim *et al.*, “Stretchable and Foldable Silicon Integrated Circuits,” *Science*, vol. 320, no. 5875, pp. 507–511, Apr. 2008, doi: 10.1126/science.1154367.

[126] S. Sankar *et al.*, “Texture discrimination with a soft biomimetic finger using a flexible neuromorphic tactile sensor array and sensory feedback,” *accepted by Soft Robotics*, Aug. 2020.

[127] L. Osborn, H. Nguyen, J. Betthauser, R. Kaliki, and N. Thakor, “Biologically inspired multi-layered synthetic skin for tactile feedback in prosthetic limbs,” in *2016 38th Annual International Conference of the IEEE Engineering in Medicine and Biology Society (EMBC)*, Orlando, FL, USA, Aug. 2016, pp. 4622–4625, doi: 10.1109/EMBC.2016.7591757.

[128] H. K. Yap, J. C. H. Goh, and R. C. H. Yeow, “Design and Characterization of Soft Actuator for Hand Rehabilitation Application,” in *6th European Conference of the International Federation for Medical and Biological Engineering*, vol. 45, I. Lacković and D. Vasic, Eds. Cham: Springer International Publishing, 2015, pp. 367–370.

[129] P. Mazza, M. Shin, and A. Santamaria, “Shape Memory Alloy As Artificial Muscles for Facial Prosthesis,” in *Volume 3: Biomedical and Biotechnology Engineering*, Tampa, Florida, USA, Nov. 2017, p. V003T04A077, doi: 10.1115/IMECE2017-71621.

[130] Y. Sun *et al.*, “Stiffness Customization and Patterning for Property Modulation of Silicone-Based Soft Pneumatic Actuators,” *Soft Robotics*, vol. 4, no. 3, pp. 251–260, Sep. 2017, doi: 10.1089/soro.2016.0047.

[131] M. J. Pearson *et al.*, “Implementing Spiking Neural Networks for Real-Time Signal-Processing and Control Applications: A Model-Validated FPGA Approach,”

IEEE Trans. Neural Netw., vol. 18, no. 5, pp. 1472–1487, Sep. 2007, doi: 10.1109/TNN.2007.891203.

[132] S.-C. Liu and T. Delbruck, "Neuromorphic sensory systems," *Current Opinion in Neurobiology*, vol. 20, no. 3, pp. 288–295, Jun. 2010, doi: 10.1016/j.conb.2010.03.007.

[133] E. M. Izhikevich, "Simple model of spiking neurons," *IEEE Trans. Neural Netw.*, vol. 14, no. 6, pp. 1569–1572, Nov. 2003, doi: 10.1109/TNN.2003.820440.

[134] M. Kuhn and K. Johnson, *Applied predictive modeling*. New York: Springer, 2013.

[135] G. James, D. Witten, T. Hastie, and R. Tibshirani, Eds., *An introduction to statistical learning: with applications in R*. New York: Springer, 2013.

[136] L. Osborn *et al.*, "Targeted transcutaneous electrical nerve stimulation for phantom limb sensory feedback," in *2017 IEEE Biomedical Circuits and Systems Conference (BioCAS)*, Torino, Oct. 2017, pp. 1–4, doi: 10.1109/BIOCAS.2017.8325200.

[137] B. R. Hunt, "Super-resolution of images: Algorithms, principles, performance," *Int. J. Imaging Syst. Technol.*, vol. 6, no. 4, pp. 297–304, 1995, doi: 10.1002/ima.1850060403.

[138] K. E. Herold and A. Rasooly, Eds., "- Micropatterned Biosensing Surfaces for Detection of Cell-Secreted Inflammatory Signals," in *Biosensors and Molecular Technologies for Cancer Diagnostics*, 0 ed., CRC Press, 2012, pp. 414–429.

[139] B. Mughal and M. Sharif, "Automated Detection of Breast Tumor in Different Imaging Modalities: A Review," *CMIR*, vol. 13, no. 2, pp. 121–139, Apr. 2017, doi: 10.2174/1573405612666160901121802.

[140] J. P. Radtke *et al.*, "Multiparametric Magnetic Resonance Imaging (MRI) and MRI–Transrectal Ultrasound Fusion Biopsy for Index Tumor Detection: Correlation with Radical Prostatectomy Specimen," *European Urology*, vol. 70, no. 5, pp. 846–853, Nov. 2016, doi: 10.1016/j.eururo.2015.12.052.

[141] J.-H. Lee, C.-H. Won, K. Yan, Y. Yu, and L. Liao, "Tactile Sensation Imaging for Artificial Palpation," in *Haptics: Generating and Perceiving Tangible Sensations*, vol. 6191, A. M. L. Kappers, J. B. F. van Erp, W. M. Bergmann Tiest, and F. C. T. van der Helm, Eds. Berlin, Heidelberg: Springer Berlin Heidelberg, 2010, pp. 373–378.

[142] N. Oestreicher, E. White, C. D. Lehman, M. T. Mandelson, P. L. Porter, and S. H. Taplin, "Predictors of Sensitivity of Clinical Breast Examination (CBE)," *Breast Cancer Res Treat*, vol. 76, no. 1, pp. 73–81, Nov. 2002, doi: 10.1023/A:1020280623807.

[143] C. Bancej, K. Decker, A. Chiarelli, M. Harrison, D. Turner, and J. Brisson, "Contribution of clinical breast examination to mammography screening in the early detection of breast cancer," *J Med Screen*, vol. 10, no. 1, pp. 16–21, 2003, doi: 10.1258/096914103321610761.

[144] R. J. B. de Jong, R. J. Rongen, J. S. Lameris, M. Harthoorn, C. D. A. Verwoerd, and P. Knegt, "Metastatic Neck Disease: Palpation vs Ultrasound Examination," *Archives of Otolaryngology - Head and Neck Surgery*, vol. 115, no. 6, pp. 689–690, Jun. 1989, doi: 10.1001/archotol.1989.01860300043013.

[145] A. Ahuja and M. Ying, “Sonography of Neck Lymph Nodes. Part II: Abnormal Lymph Nodes,” *Clinical Radiology*, vol. 58, no. 5, pp. 359–366, May 2003, doi: 10.1016/S0009-9260(02)00585-8.

[146] J. A. Castelijns and M. W. M. van den Brekel, “Neck Nodal Disease,” in *Head and Neck Cancer Imaging*, R. Hermans, Ed. Berlin, Heidelberg: Springer Berlin Heidelberg, 2006, pp. 293–309.

[147] Q. Wing-Han Yuen, “In-vitro Strain and Modulus Measurements in Porcine Cervical Lymph Nodes,” *TOBEJ*, vol. 5, no. 1, pp. 39–46, Mar. 2011, doi: 10.2174/1874120701105010039.

[148] “Tissue Analytics.” https://www.tissue-analytics.com/#page=wound_management.

[149] “Wound Works.” https://woundworks.com/technology-3d-wound-imaging/.

[150] R. “Sal” Salcido, “Beyond Photography: Wound Imaging,” *Advances in Skin & Wound Care*, vol. 24, no. 2, p. 56, Feb. 2011, doi: 10.1097/01.ASW.0000393763.33808.32.

[151] X. Xiao, B. Gao, G. Y. Tian, Y. C. Zhang, and S. Chen, “Novel Ultrasound System With Intelligent Compensation for High Precision Measurement of Thin Wall Tube,” *IEEE Sensors J.*, vol. 18, no. 16, pp. 6633–6643, Aug. 2018, doi: 10.1109/JSEN.2018.2826547.

[152] R. H. Silverman, “High-resolution ultrasound imaging of the eye - a review,” *Clinical & Experimental Ophthalmology*, vol. 37, no. 1, pp. 54–67, Jan. 2009, doi: 10.1111/j.1442-9071.2008.01892.x.

[153] K. Ohtani, M. Baba, and T. Konishi, "Position and posture measurements and shape recognition of columnar objects using an ultrasonic sensor array and neural networks," *Syst. Comp. Jpn.*, vol. 33, no. 11, pp. 27–38, Oct. 2002, doi: 10.1002/scj.10103.

[154] S. Zhang, J. Chen, and S. He, "Novel ultrasound detector based on small slot micro-ring resonator with ultrahigh Q factor," *Optics Communications*, vol. 382, pp. 113–118, Jan. 2017, doi: 10.1016/j.optcom.2016.07.082.

[155] H. Kim *et al.*, "Miniature ultrasound ring array transducers for transcranial ultrasound neuromodulation of freely-moving small animals," *Brain Stimulation*, vol. 12, no. 2, pp. 251–255, Mar. 2019, doi: 10.1016/j.brs.2018.11.007.

[156] W. Heeman, W. Steenbergen, G. M. van Dam, and E. C. Boerma, "Clinical applications of laser speckle contrast imaging: a review," *J. Biomed. Opt.*, vol. 24, no. 08, p. 1, Aug. 2019, doi: 10.1117/1.JBO.24.8.080901.

[157] E. Biddiss and T. Chau, "Upper-Limb Prosthetics: Critical Factors in Device Abandonment," *American Journal of Physical Medicine & Rehabilitation*, vol. 86, no. 12, pp. 977–987, Dec. 2007, doi: 10.1097/PHM.0b013e3181587f6c.

[158] A. E. Schultz, S. P. Baade, and T. A. Kuiken, "Expert opinions on success factors for upper-limb prostheses," *JRRD*, vol. 44, no. 4, p. 483, 2007, doi: 10.1682/JRRD.2006.08.0087.

[159] B. E. Stein, T. R. Stanford, and B. A. Rowland, "Development of multisensory integration from the perspective of the individual neuron," *Nat. Rev. Neurosci.*, vol. 15, no. 8, pp. 520–535, Aug. 2014, doi: 10.1038/nrn3742.

[160] M. S. Beauchamp, B. D. Argall, J. Bodurka, J. H. Duyn, and A. Martin, "Unraveling multisensory integration: patchy organization within human STS multisensory cortex," *Nat Neurosci*, vol. 7, no. 11, pp. 1190–1192, Nov. 2004, doi: 10.1038/nn1333.

[161] B. De Gelder and P. Bertelson, "Multisensory integration, perception and ecological validity," *Trends in Cognitive Sciences*, vol. 7, no. 10, pp. 460–467, Oct. 2003, doi: 10.1016/j.tics.2003.08.014.

[162] T. Ohshiro, D. E. Angelaki, and G. C. DeAngelis, "A normalization model of multisensory integration," *Nat Neurosci*, vol. 14, no. 6, pp. 775–782, Jun. 2011, doi: 10.1038/nn.2815.

[163] W. P. Chan *et al.*, "Multimodal sensing and active continuous closed-loop feedback for achieving reliable manipulation in the outdoor physical world: CHAN ET AL.," *J Field Robotics*, vol. 36, no. 1, pp. 17–33, Jan. 2019, doi: 10.1002/rob.21818.

[164] S. Park, C. Meeker, L. M. Weber, L. Bishop, J. Stein, and M. Ciocarlie, "Multimodal Sensing and Interaction for a Robotic Hand Orthosis," *IEEE Robot. Autom. Lett.*, vol. 4, no. 2, pp. 315–322, Apr. 2019, doi: 10.1109/LRA.2018.2890199.

[165] D. Watkins-Valls, J. Varley, and P. Allen, "Multi-Modal Geometric Learning for Grasping and Manipulation," in *2019 International Conference on Robotics and Automation (ICRA)*, Montreal, QC, Canada, May 2019, pp. 7339–7345, doi: 10.1109/ICRA.2019.8794233.

[166] Z. Li, J. Deng, R. Lu, Y. Xu, J. Bai, and C.-Y. Su, "Trajectory-Tracking Control of Mobile Robot Systems Incorporating Neural-Dynamic Optimized Model Predictive

Approach," *IEEE Trans. Syst. Man Cybern, Syst.*, vol. 46, no. 6, pp. 740–749, Jun. 2016, doi: 10.1109/TSMC.2015.2465352.

[167] F. S. S. Leijten and the Dutch TeleEpilepsy Consortium, "Multimodal seizure detection: A review," *Epilepsia*, vol. 59, pp. 42–47, Jun. 2018, doi: 10.1111/epi.14047.

[168] C. Diaz and S. Payandeh, "Multimodal Sensing Interface for Haptic Interaction," *Journal of Sensors*, vol. 2017, pp. 1–24, 2017, doi: 10.1155/2017/2072951.

[169] K. Yu, Ed., *Positioning and Navigation in Complex Environments:* IGI Global, 2018.

[170] A. Asadipour, K. Debattista, V. Patel, and A. Chalmers, "A technology-aided multi-modal training approach to assist abdominal palpation training and its assessment in medical education," *International Journal of Human-Computer Studies*, vol. 137, p. 102394, May 2020, doi: 10.1016/j.ijhcs.2020.102394.

[171] A. Escoto *et al.*, "A multi-sensory mechatronic device for localizing tumors in minimally invasive interventions," in *2015 IEEE International Conference on Robotics and Automation (ICRA)*, Seattle, WA, USA, May 2015, pp. 4742–4747, doi: 10.1109/ICRA.2015.7139858.

[172] V. A. Knyaz, "Multimodal data fusion for object recognition," in *Multimodal Sensing: Technologies and Applications*, Munich, Germany, Jun. 2019, p. 19, doi: 10.1117/12.2526067.

[173] Y. Lu, G. Lu, X. Bu, Y. Yu, and X. Bu, "Classification of Hand Manipulation Using BP Neural Network and Support Vector Machine Based on Surface

Electromyography Signal," *IFAC-PapersOnLine*, vol. 48, no. 28, pp. 869–873, 2015, doi: 10.1016/j.ifacol.2015.12.239.

[174] Y. Xue, Z. Ju, K. Xiang, J. Chen, and H. Liu, "Multimodal Human Hand Motion Sensing and Analysis—A Review," *IEEE Trans. Cogn. Dev. Syst.*, vol. 11, no. 2, pp. 162–175, Jun. 2019, doi: 10.1109/TCDS.2018.2800167.

[175] P. Hebert, N. Hudson, J. Ma, and J. W. Burdick, "Dual arm estimation for coordinated bimanual manipulation," in *2013 IEEE International Conference on Robotics and Automation*, Karlsruhe, Germany, May 2013, pp. 120–125, doi: 10.1109/ICRA.2013.6630565.

[176] M. Prats, P. Martinet, A. P. del Pobil, and S. Lee, "Robotic execution of everyday tasks by means of external vision/force control," *Intel Serv Robotics*, vol. 1, no. 3, pp. 253–266, Jul. 2008, doi: 10.1007/s11370-007-0008-x.

[177] M. Prats, P. J. Sanz, and A. P. del Pobil, "Reliable non-prehensile door opening through the combination of vision, tactile and force feedback," *Auton Robot*, vol. 29, no. 2, pp. 201–218, Aug. 2010, doi: 10.1007/s10514-010-9192-1.

[178] P. Hebert, N. Hudson, J. Ma, and J. Burdick, "Fusion of stereo vision, force-torque, and joint sensors for estimation of in-hand object location," in *2011 IEEE International Conference on Robotics and Automation*, Shanghai, China, May 2011, pp. 5935–5941, doi: 10.1109/ICRA.2011.5980185.

[179] I. Kumagai *et al.*, "Achievement of localization system for humanoid robots with virtual horizontal scan relative to improved odometry fusing internal sensors and visual information," in *2016 IEEE/RSJ International Conference on Intelligent*

Robots and Systems (IROS), Daejeon, South Korea, Oct. 2016, pp. 666–673, doi: 10.1109/IROS.2016.7759124.

[180] W. W. Lee *et al.*, "A neuro-inspired artificial peripheral nervous system for scalable electronic skins," *Sci Robot.*, vol. 4, no. 32, p. eaax2198, Jul. 2019, doi: 10.1126/scirobotics.aax2198.

[181] D. Kumar, R. Ghosh, A. Nakagawa-Silva, A. B. Soares, and N. V. Thakor, "Neuromorphic Approach to Tactile Edge Orientation Estimation using Spatiotemporal Similarity," *Neurocomputing*, p. S0925231220307785, May 2020, doi: 10.1016/j.neucom.2020.04.131.

[182] W. W. Lee, S. L. Kukreja, and N. V. Thakor, "A kilohertz kilotaxel tactile sensor array for investigating spatiotemporal features in neuromorphic touch," in *2015 IEEE Biomedical Circuits and Systems Conference (BioCAS)*, Atlanta, GA, USA, Oct. 2015, pp. 1–4, doi: 10.1109/BioCAS.2015.7348412.

Vita

Sriramana Sankar received his Bachelor of Science degree in Biological Systems Engineering from Kansas State University in 2014. He continued his education at Johns Hopkins University's Biomedical Engineering MSE program. His research focused on developing soft upper-limb prosthesis and flexible sensing for texture discrimination applications. He has been a Teaching Assistant in the Principles of Biomedical Instrumentation course offered at JHU. His work has been accepted by the Soft Robotics journal, has been presented at the 2019 IEEE Sensors conference, and is under review by the Annals in Biomedical Engineering journal.